15 Boniface, K., Bernard, F. X., Garcia, M., Gurney, A. L., Lecron, J. C. and Morel, F., IL-22 inhibits epidermal differentiation and induces pro-inflammatory gene expression and migration of human keratinocytes. *J. Immunol.* 2005. **174**: 3695–3702.

16 Kotenko, S. V., Izotova, L. S., Mirochnitchenko, O. V., Esterova, E., Dickensheets, H., Donnelly, R. P. and Pestka, S., Identification of the functional interleukin-22 (IL-22) receptor complex: the IL-10R2 chain (IL-10Rbeta) is a common chain of both the IL-10 and IL-22 (IL-10-related T cell-derived inducible factor, IL-TIF) receptor complexes. *J. Biol. Chem.* 2001. **276**: 2725–2732.

17 Kunz, S., Wolk, K., Witte, E., Witte, K., Doecke, W. D., Volk, H. D., Sterry, W. *et al.*, Interleukin (IL)-19, IL-20 and IL-24 are produced by and act on keratinocytes and are distinct from classical ILs. *Exp. Dermatol.* 2006. **15**: 991–1004.

18 Nagalakshmi, M. L., Murphy, E., McClanahan, T. and de Waal Malefyt, R., Expression patterns of IL-10 ligand and receptor gene families provide leads for biological characterization. *Int. Immunopharmacol.* 2004. **4**: 577–592.

19 Wolk, K., Kunz, S., Asadullah, K. and Sabat, R., Cutting edge: immune cells as sources and targets of the IL-10 family members? *J. Immunol.* 2002. **168**: 5397–5402.

20 Huang, F., Wachi, S., Thai, P., Loukoianov, A., Tan, K. H., Forteza, R. M. and Wu, R., Potentiation of IL-19 expression in airway epithelia by IL-17A and IL-4/IL-13: important implications in asthma. *J. Allergy Clin. Immunol.* 2008. **121**: 1415–1421, 1421 e1–3.

21 Pestka, S., Krause, C. D., Sarkar, D., Walter, M. R., Shi, Y. and Fisher, P. B., Interleukin-10 and related cytokines and receptors. *Annu. Rev. Immunol.* 2004. **22**: 929–979.

22 Dumoutier, L., Leemans, C., Lejeune, D., Kotenko, S. V. and Renauld, J. C., Cutting edge: STAT activation by IL-19, IL-20 and mda-7 through IL-20 receptor complexes of two types. *J. Immunol.* 2001. **167**: 3545–3549.

23 Parrish-Novak, J., Xu, W., Brender, T., Yao, L., Jones, C., West, J., Brandt, C. *et al.*, Interleukins 19, 20, and 24 signal through two distinct receptor complexes. Differences in receptor-ligand interactions mediate unique biological functions. *J. Biol. Chem.* 2002. **277**: 47517–47523.

24 Sano, S., Chan, K. S., Carbajal, S., Clifford, J., Peavey, M., Kiguchi, K., Itami, S. *et al.*, Stat3 links activated keratinocytes and immunocytes required for development of psoriasis in a novel transgenic mouse model. *Nat. Med.* 2005. **11**: 43–49.

25 Romer, J., Hasselager, E., Norby, P. L., Steiniche, T., Thorn Clausen, J. and Kragballe, K., Epidermal overexpression of interleukin-19 and -20 mRNA in psoriatic skin disappears after short-term treatment with cyclosporine a or calcipotriol. *J. Invest. Dermatol.* 2003. **121**: 1306–1311.

26 Otkjaer, K., Kragballe, K., Funding, A. T., Clausen, J. T., Noerby, P. L., Steiniche, T. and Iversen, L., The dynamics of gene expression of interleukin-19 and interleukin-20 and their receptors in psoriasis. *Br. J. Dermatol.* 2005. **153**: 911–918.

27 Gallagher, G., Dickensheets, H., Eskdale, J., Izotova, L. S., Mirochnitchenko, O. V., Peat, J. D., Vazquez, N. *et al.*, Cloning, expression and initial characterization of interleukin-19 (IL-19), a novel homologue of human interleukin-10 (IL-10). *Genes Immun.* 2000. **1**: 442–450.

28 Poindexter, N. J., Walch, E. T., Chada, S. and Grimm, E. A., Cytokine induction of interleukin-24 in human peripheral blood mononuclear cells. *J. Leukoc. Biol.* 2005. **78**: 745–752.

29 Wolk, K., Witte, K., Witte, E., Proesch, S., Schulze-Tanzil, G., Nasilowska, K., Thilo, J. *et al.*, Maturing dendritic cells are an important source of IL-29 and IL-20 that may cooperatively increase the innate immunity of keratinocytes. *J. Leukoc. Biol.* 2008. **83**: 1181–1193.

30 Wang, F., Lee, E., Lowes, M. A., Haider, A. S., Fuentes-Duculan, J., Abello, M. V., Chamian, F. *et al.*, Prominent production of IL-20 by $CD68^+/CD11c^+$ myeloid-derived cells in psoriasis: gene regulation and cellular effects. *J. Invest. Dermatol.* 2006. **126**: 1590–1599.

31 Liang, S. C., Tan, X. Y., Luxenberg, D. P., Karim, R., Dunussi-Joannopoulos, K., Collins, M. and Fouser, L. A., Interleukin (IL)-22 and IL-17 are coexpressed by Th17 cells and cooperatively enhance expression of antimicrobial peptides. *J. Exp. Med.* 2006. **203**: 2271–2279.

32 Jiang, H., Lin, J. J., Su, Z. Z., Goldstein, N. I. and Fisher, P. B., Subtraction hybridization identifies a novel melanoma differentiation associated gene, mda-7, modulated during human melanoma differentiation, growth and progression. *Oncogene* 1995. **11**: 2477–2486.

33 Wilson, N. J., Boniface, K., Chan, J. R., McKenzie, B. S., Blumenschein, W. M., Mattson, J. D., Basham, B. *et al.*, Development, cytokine profile and function of human interleukin 17-producing helper T cells. *Nat. Immunol.* 2007. **8**: 950–957.

34 Annunziato, F., Cosmi, L., Santarlasci, V., Maggi, L., Liotta, F., Mazzinghi, B., Parente, E. *et al.*, Phenotypic and functional features of human Th17 cells. *J. Exp. Med.* 2007. **204**: 1849–1861.

35 Singh, S. P., Zhang, H. H., Foley, J. F., Hedrick, M. N. and Farber, J. M., Human T cells that are able to produce IL-17 express the chemokine receptor CCR6. *J. Immunol.* 2008. **180**: 214–221.

36 Hashimoto, K., Higashiyama, S., Asada, H., Hashimura, E., Kobayashi, T., Sudo, K., Nakagawa, T. *et al.*, Heparin-binding epidermal growth factor-like growth factor is an autocrine growth factor for human keratinocytes. *J. Biol. Chem.* 1994. **269**: 20060–20066.

37 Boniface, K., Guignouard, E., Pedretti, N., Garcia, M., Delwail, A., Bernard, F. X., Nau, F. *et al.*, A role for T cell-derived interleukin 22 in psoriatic skin inflammation. *Clin. Exp. Immunol.* 2007. **150**: 407–415.

38 Liao, S. C., Cheng, Y. C., Wang, Y. C., Wang, C. W., Yang, S. M., Yu, C. K., Shieh, C. C. *et al.*, IL-19 induced Th2 cytokines and was up-regulated in asthma patients. *J. Immunol.* 2004. **173**: 6712–6718.

39 Gallagher, G., Eskdale, J., Jordan, W., Peat, J., Campbell, J., Boniotto, M., Lennon, G. P. *et al.*, Human interleukin-19 and its receptor: a potential role in the induction of Th2 responses. *Int. Immunopharmacol.* 2004. **4**: 615–626.

40 Hsing, C. H., Hsu, C. C., Chen, W. Y., Chang, L. Y., Hwang, J. C. and Chang, M. S., Expression of IL-19 correlates with Th2 cytokines in uraemic patients. *Nephrol. Dial. Transplant.* 2007. **22**: 2230–2238.

41 Shirakata, Y., Ueno, H., Hanakawa, Y., Kameda, K., Yamasaki, K., Tokumaru, S., Yahata, Y. *et al.*, TGF-beta is not involved in early phase growth inhibition of keratinocytes by 1alpha,25(OH)2vitamin D3. *J. Dermatol. Sci.* 2004. **36**: 41–50.

42 Hanakawa, Y., Amagai, M., Shirakata, Y., Sayama, K. and Hashimoto, K., Different effects of dominant negative mutants of desmocollin and desmoglein on the cell-cell adhesion of keratinocytes. *J. Cell. Sci.* 2000. **113**: 1803–1811.

Abbreviations: **Ax:** adenovirus vector · **AxIL22R:** Ax carrying IL-22R · **HBD2:** human beta-defensin 2 · **HB-EGF:** heparin-binding EGF-like growth factor

Full correspondence: Dr. Mikiko Tohyama, Department of Dermatology, Ehime University Graduate School of Medicine, Toon-city, Ehime 791-0295, Japan
Fax: +81-89-960-5352
e-mail: tohm@m.ehime-u.ac.jp

Received: 31/3/2009
Revised: 26/6/2009
Accepted: 7/7/2009

Journal of Dermatological Science 56 (2009) 188–195

Contents lists available at ScienceDirect

Journal of Dermatological Science

journal homepage: www.intl.elsevierhealth.com/journals/jods

Living skin equivalents constructed using human amnions as a matrix

Lujun Yang[1], Yuji Shirakata[1,*], Sho Tokumaru, Dai Xiuju, Mikiko Tohyama, Yasushi Hanakawa, Satoshi Hirakawa, Koji Sayama, Koji Hashimoto

Department of Dermatology, Ehime University Graduate School of Medicine, Shitsukawa 454, Toon City, Ehime, 791-0295, Japan

ARTICLE INFO

Article history:
Received 17 July 2009
Received in revised form 24 September 2009
Accepted 24 September 2009

Keywords:
Amnion
Living skin equivalent
Mesenchymal interaction
Basement membrane

ABSTRACT

Background: Living skin equivalents (LSEs) are being used to treat burn wounds, skin defects, and chronic wounds, and today, several biomaterials are applied as dermal matrices in LSEs. The amnionic membrane (AM) is known to have useful properties as a dermal matrix and can be used to construct a LSE.
Objective: To develop a new LSE with human AM as the matrix.
Methods: Human AM was de-epithelialized and investigated to determine whether it supported keratinocyte adherence and proliferation, and fibroblast in-growth and proliferation. A new LSE was constructed by seeding keratinocytes on the epithelial side of fibroblast-populated, de-epithelialized AM and was investigated histologically. The LSE was transplanted onto a full-thickness wound on a nude mouse and a histological examination was conducted.
Results: De-epithelialized AM supported the adherence and proliferation of keratinocytes and the in-growth of fibroblasts. The new LSE demonstrated good mechanical properties and revealed good morphology, with a well differentiated epidermis and well developed basement membrane. The LSE grafts survived well on nude mice, showing good morphology.
Conclusion: A LSE with amnions as a matrix exhibited good morphology, low cost, and good mechanical properties and may be useful as a skin substitute for clinical use.

1. Introduction

Living skin equivalents (LSEs) containing well differentiated keratinocytes cultivated on fibroblast-populated dermal substitutes have been used to treat burn wounds, skin defects, chronic wounds, and ulcers [1–3]. The dermal matrix and the fibroblasts in LSEs modulate epidermal growth and differentiation through dynamic interactions [4–6]. Various biomaterials have been used as dermal matrix substitutes, including type I collagen, acellular human dermis, collagen–glycosaminoglycan matrix, human plasma, and fibrin glue [7–11]. However, the search has continued for an ideal matrix that is readily available and inexpensive and supports mesenchymal cell in-growth, improves epidermal cell adherence and proliferation, and has minimal toxicity, low immunogenicity, and good mechanical properties.

Amnions can be readily obtained from cesarean deliveries after screening for viral diseases. Amnions have been used to cover clean partial-thickness wounds and donor sites, and applied as a temporary dressing for freshly excised burns; it has advantages such as pain relief, prevention of infection, maintenance of a moist environment to promote healing, good adherence to wounds, and simple handling [12–17]. Laboratory investigations have revealed that the basement membrane (BM) of amnions shares major BM components with human skin, and the BM zone resembles human skin both morphologically and ultrastucturally [18]. The epithelial side of denuded amnions has been shown to support the proliferation, spreading, and differentiation of corneal, mucous, and bronchial epithelial cells [19–21]. Furthermore, the stroma of amnions can serve as a dermal matrix in which fibroblasts show good adherence and proliferation [22,23]. Limited immunogenicity, along with anti-inflammatory effects and other characteristics, make it a suitable transplantation material for ocular surface reconstruction, and the immune privilege of the amnion makes it a biological immune barrier for xenotransplantation [24–26]. Moreover, amnion procurement and processing are easy and it can be sterilized and preserved at low cost for long periods without obvious architectural changes [27–29].

Considering these characteristics of amnions, in this study, we used amnions as a substratum to construct a LSE. We studied the

* Corresponding author. Tel.: +81 89 960 5350; fax: +81 89 960 5352.
E-mail address: shirakat@m.ehime-u.ac.jp (Y. Shirakata).
[1] Both these authors contributed equally to this work.

0923-1811/$36.00
doi:10.1016/j.jdermsci.2009.09.009

morphology and function of fibroblasts cultured in the stroma of amnions and the morphology of keratinocytes on the epithelial side of de-epithelialized amnions. The LSE was constructed by seeding keratinocytes on fibroblast-infiltrated amnions and was investigated histologically, immunohistochemically, and ultrastructually. The LSE was also investigated *in vivo* by transplantation onto nude mice.

2. Materials and methods

2.1. Cell culture

Normal human epidermal keratinocytes (NHKs) were isolated from healthy human skin and cultured under serum-free conditions, as described previously [30,31]. The cells were used for LSE cultures in their fourth passage. Fibroblasts were isolated from healthy human skin and cultured in Dulbecco's modified Eagle's medium (DMEM; Gibco, Grand Island, NY, USA) supplemented with 10% fetal calf serum (FCS). Fifth-passage cells were used to construct the LSEs.

All procedures that involved human subjects received prior approval from the ethics committee of Ehime University School of Medicine, Toon City, Ehime, Japan. All subjects provided written informed consent.

2.2. Preparation of de-epithelialized amnions

Human amniotic membrane (AM) was obtained at cesarean section. Under sterile conditions, the AM was washed with sterile phosphate-buffered saline (PBS), deprived of the spongy layer, and stored at −80 °C in 12% dimethyl sulfoxide (DMSO) in PBS. Before use, the AM was thawed, washed with PBS three times, and cut into 2.5 cm × 2.5 cm pieces. The epithelial cells were removed from the AM by incubating it in 0.02% ethylenediaminetetraacetic acid (EDTA) at 37 °C for 2 h, and then gently scraping with a cell scraper under a microscope, as previously described [32]. The complete removal of epithelial cells was confirmed using hematoxylin and eosin (H&E) staining.

2.3. De-epithelialized AM for cultivating keratinocytes and dermal fibroblasts

De-epithelialized AM was put on the bottom of a six-well culture plate (Costar; Corning, Corning, NY, USA) with the epithelial side upward, and stabilized by overlaying a stainless steel ring (inner diameter, 20 mm). Keratinocytes (1×10^6 cells) were seeded onto the AM in MCDB 153 II medium. The same number of keratinocytes was seeded in a type I collagen-coated six-well plate (Iwaki; Asahi Techno Glass, Chiba, Japan) of the same area as the AM. Then, 4 h later, the cells were stained with calcein AM (using the Live/Dead Viability/Cytotoxicity Kit; Molecular Probes, Eugene, OR, USA) according to the manufacturer's protocol. The fluorescence was examined and photographed under a phase-contrast microscope (TE-300; Nikon, Tokyo, Japan), coupled with a Nikon pixera digital camera penguin 600 CL. Three days later, the confluent keratinocytes were photographed under the same phase-contrast microscope.

Fibroblasts (5×10^5) were seeded in each well of a six-well culture plate in DMEM supplemented with 10% FCS and 50 μg/mL ascorbic acid. When the cells reached confluence, de-epithelialized AM was placed on the cells, with the stromal side downward, to be in touch with the fibroblasts. The AM was stabilized with a stainless steel ring. At the first and fifth day after AM application, pictures were taken of the fibroblasts on the AM.

We performed at least three independent experiments, which showed similar results. Representative data are shown in the figures.

2.4. Preparation of skin equivalents

Fibroblasts (5×10^5) were seeded in culture inserts (Transwell-COL, membrane pore size, 3 μm, Costar; Corning) and cultured in DMEM supplemented with 10% FCS in a 6-well plate (Costar; Corning). One day later, de-epithelialized AM was put on to the confluent fibroblasts, with the stromal side downward, and stabilized with a stainless steel ring (inner diameter, 20 mm). Five days later, when the fibroblasts had infiltrated the AM stroma (confirmed by phase-contrast microscopy), 2×10^6 keratinocytes in 500 μL MCDB 153 type II medium were seeded in the hole of the stainless steel ring. The keratinocytes were kept submerged in culture for 2 days. Then, the LSE was lifted to provide an air–liquid interface and cornification medium (1:1 mixture of Ham's F-12 and DMEM supplemented with 2% FCS and other supplements, as described previously [33]) was added. This medium was changed every other day.

The LSEs were harvested at day 10 after airlift. For each sample, one part was fixed in 20% formalin and embedded in paraffin for H&E staining, one part was snap-frozen in optimal cutting temperature (OCT) compound for immunofluorescence staining, and one small part was processed for transmission electronic microscopy (TEM). We performed more than 20 experiments, and similar results were obtained. A representative experiment is shown in the figures.

2.5. Histology and immunofluorescence staining

Paraffin-embedded LSE samples were sectioned at 6 μm and stained with H&E. Images were obtained using an Olympus AX80 microscope coupled with an Olympus DP50 digital camera (Olympus, Tokyo, Japan).

For immunofluorescence (IF) staining, frozen sections (7 μm) were first incubated with 0.3% hydrogen peroxide for 30 min to remove endogenous peroxidase activity and then incubated with primary antibodies at appropriate dilutions (Table 1) overnight at 4 °C. The sections were incubated with anti-mouse fluorescein isothiocyanate (FITC) for 30 min at room temperature. Images were obtained using a fluorescence microscope (E6TUW-RFL; Nikon) coupled with an Olympus DP70 digital camera. We performed at least three independent studies, which gave similar results. A representative experiment is shown in the figures.

2.6. Mechanical and handling properties of the living skin equivalent and transplantation on nude mice

A larger LSE was made using a larger culture insert (diameter, 75 mm, membrane pore size, 3 μm, Transwell; Corning), a larger piece of amnions (about 4 cm × 4 cm), and proportionally more fibroblasts and keratinocytes in the same way as described above. At day 7 after airlift, the LSE was harvested and made into a mesh-skin graft with a scalpel and stretched.

The grafting protocol was approved by the ethics committee of Ehime University School of Medicine. Eight-week-old female

Table 1
Details of primary antibodies.

Antibody to	Clone	Dilution	Source
E-cadherin	HECD-1	1:100	TaKaRa
Desmoglein 3	5G11	1:100	Zymed
Keratin 14	LL002	1:100	NeoMarkers
Keratin 10	LHP1	1:100	NeoMarkers
Integrin β4	3E1	1:100	Chemicon
Integrin α2	P1E6	1:100	Chemicon
Collagen type VII	LH7.2	1:100	NeoMarkers
Collagen type IV	2311C3	1:200	Chemicon
Laminin 5	GB3	1:100	Sera-lab

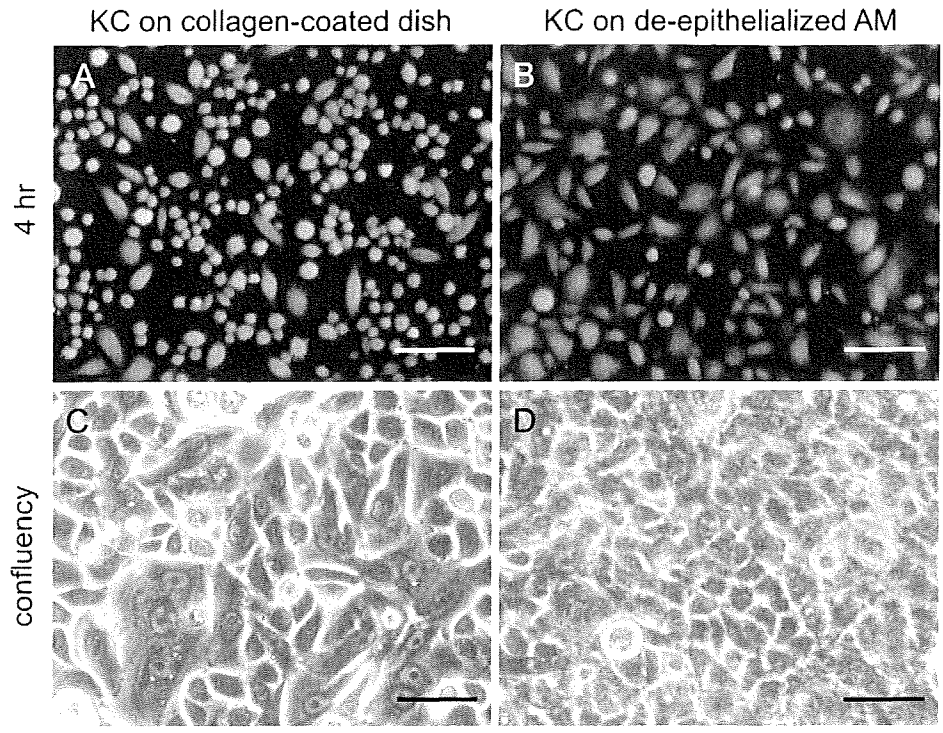

Fig. 1. Morphology of keratinocytes on de-epithelialized amnions. Keratinocytes were seeded onto a type I collagen-coated dish (A and C) or the epidermal side of de-epithelialized amnions (B and D). Four hours after seeding, the plasma of cells was stained with calcein AM of the Live/Dead Viability/Cytotoxicity Kit and photographed (A and B). Three days later, the cells reached confluence and were photographed under a phase-contrast microscope (C and D). Bars are 50 μm.

BALB/cAJc1-nu nude mice were anesthetized with intraperitoneal injection of 0.3 mL Avertin (1.25% tribromoethanol, 2.5% 2-methyl-2-butanol solution). A 1.5 cm × 1.5 cm full-thickness wound was created on the back of each mouse using scissors; then a piece of LSE of matching size (7 days after airlift) was grafted onto the wound and covered with a transparent film. Fourteen days after transplantation, pictures of the grafts were taken and the grafts were harvested and processed for H&E staining. We performed at least three independent studies, which gave similar results. A representative experiment is shown in the figures.

2.7. Transmission electron microscopy

Specimens were fixed in 0.1% tannic acid containing 2.5% glutaraldehyde in 0.1 M phosphate buffer (pH 7.4) for 2 h, washed with phosphate buffer, post-fixed with 1% osmium tetroxide in phosphate buffer for 2 h, washed with 0.25 M sucrose solution, dehydrated in a graded series of ethanols, and embedded in an Epon resin mixture. Ultrathin sections (<60–80 nm) were prepared using an Ultracut S (Leica, Solms, Germany) double-stained with uranyl acetate and lead citrate, and examined with a

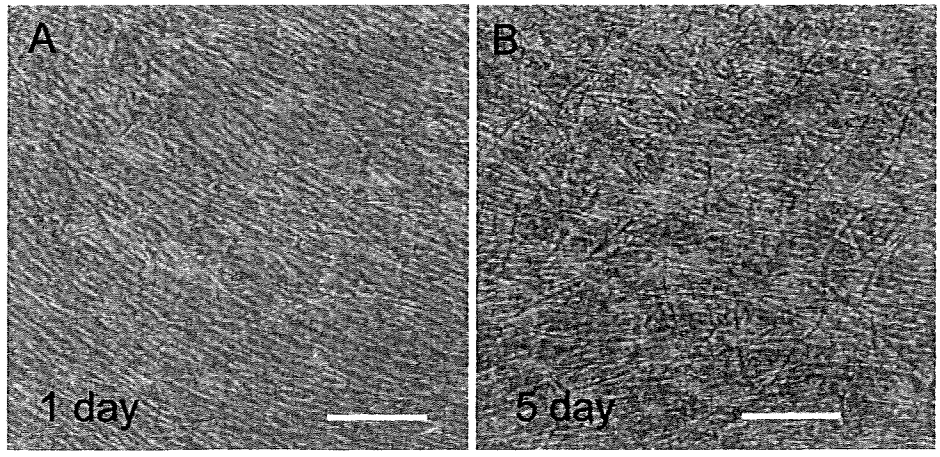

Fig. 2. Morphology of fibroblasts in the stroma of amnions. De-epithelialized amnions were placed on confluent fibroblasts with the stromal side downward. One day (A) or 5 days (B) later, the morphology of fibroblasts was examined. Bars are 50 μm.

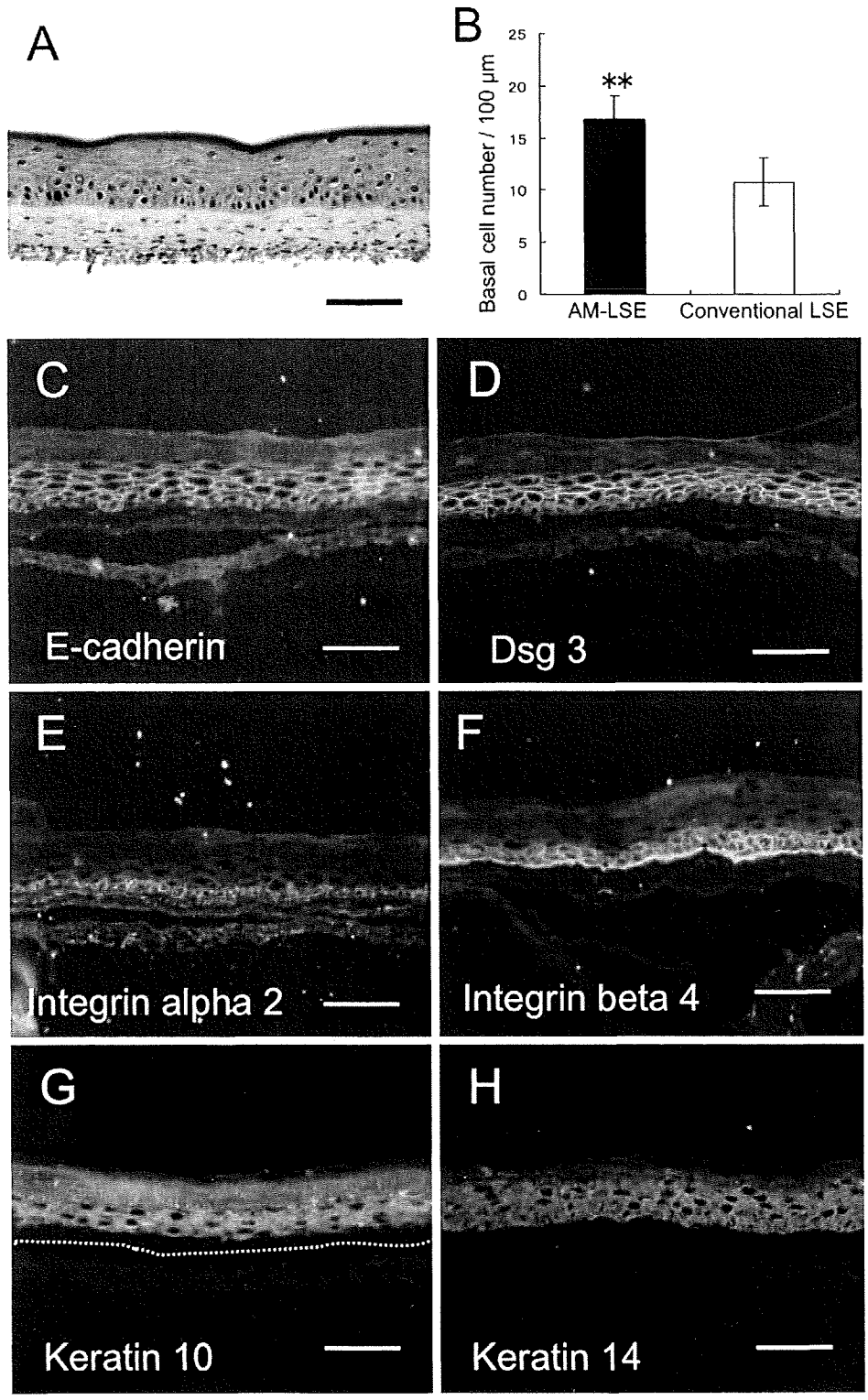

Fig. 3. Morphology of living skin equivalents and the expression of cell–cell junction proteins, integrins, and keratins. Keratinocytes were seeded onto fibroblast-infiltrated de-epithelialized amnions to create living skin equivalents (LSEs). Ten days after airlift, the LSEs were harvested. The histological morphology is indicated by H&E staining (A). The basal cell number per 100 μm at dermal-epidermal junction was counted, and compared with a conventional LSE built with type I collagen. $^{**}p < 0.05$ (B). The cell–cell junction is shown by immunofluorescence (IF) staining of E-cadherin (C) and Dsg 3 (D). The polarization of epidermal cells is indicated by IF staining of integrin α2 (E) and β4 (F). The differentiation and proliferation status of the epidermis are shown by the expressions of keratin 10 (G) and keratin 14 (H). Bars are 50 μm.

transmission electron microscope (JEM-1230; JEOL, Tokyo, Japan) at 80 kV. We performed at least three independent studies and confirmed similar results. A representative experiment is shown in the figures.

3. Results

3.1. De-epithelialized amnions supported keratinocyte and fibroblast growth

Four hours after the seeding of keratinocytes, the cell plasma was stained with calcein AM and the morphology of the keratinocytes was observed. In amnions, most of the cells became larger and adopted a spindle-like shape (Fig. 1B) in comparison with the small and round cells on the type I collagen-coated dish (Fig. 1A). At day 3, when the cells reached confluence, keratinocytes on de-epithelialized amnions appeared more compactly arranged with a pavement stonelike morphology (Fig. 1D), while the cells on the type I collagen were larger and appeared irregular (Fig. 1C).

The amnions were overlaid with the stromal side downward on confluent fibroblasts. Under phase-contrast microscopy, we observed morphological changes in the fibroblasts in the amnions. One day after amnion application, very few fibroblasts sprouted into the amnions, with thin and long dendritic branches (Fig. 2A). At day 5, more fibroblasts moved into the stroma of the amnions and formed a complex network of dendritic branches (Fig. 2B).

3.2. A well differentiated epidermis formed on de-epithelialized amnion with a well developed basement membrane

At day 10 after airlift, the LSEs were harvested and processed for histological, immunohistochemical, and ultrastructural studies. A multilayered epidermis formed on de-epithelialized amnions and epidermal stratification was well organized (Fig. 3A). The basal cells were cuboid, small, and compactly aligned along the AM, with clear demarcation. The number of basal cells on dermal–epidermal junction is significantly higher than that of a conventional LSE made by seeding keratinocytes on fibroblast-populated type I collagen gel (Fig. 3B) [32,33]. The spinous layer, granular layer, and stratum corneum were also clearly identified. The fibroblasts infiltrated deeply into the stroma of the amnion except for a thin acellular zone, which separated the epidermis from the underlying fibroblast-infiltrated substratum (Fig. 3A). Cell–cell junctions were well developed in the epidermis, as shown by the expression of

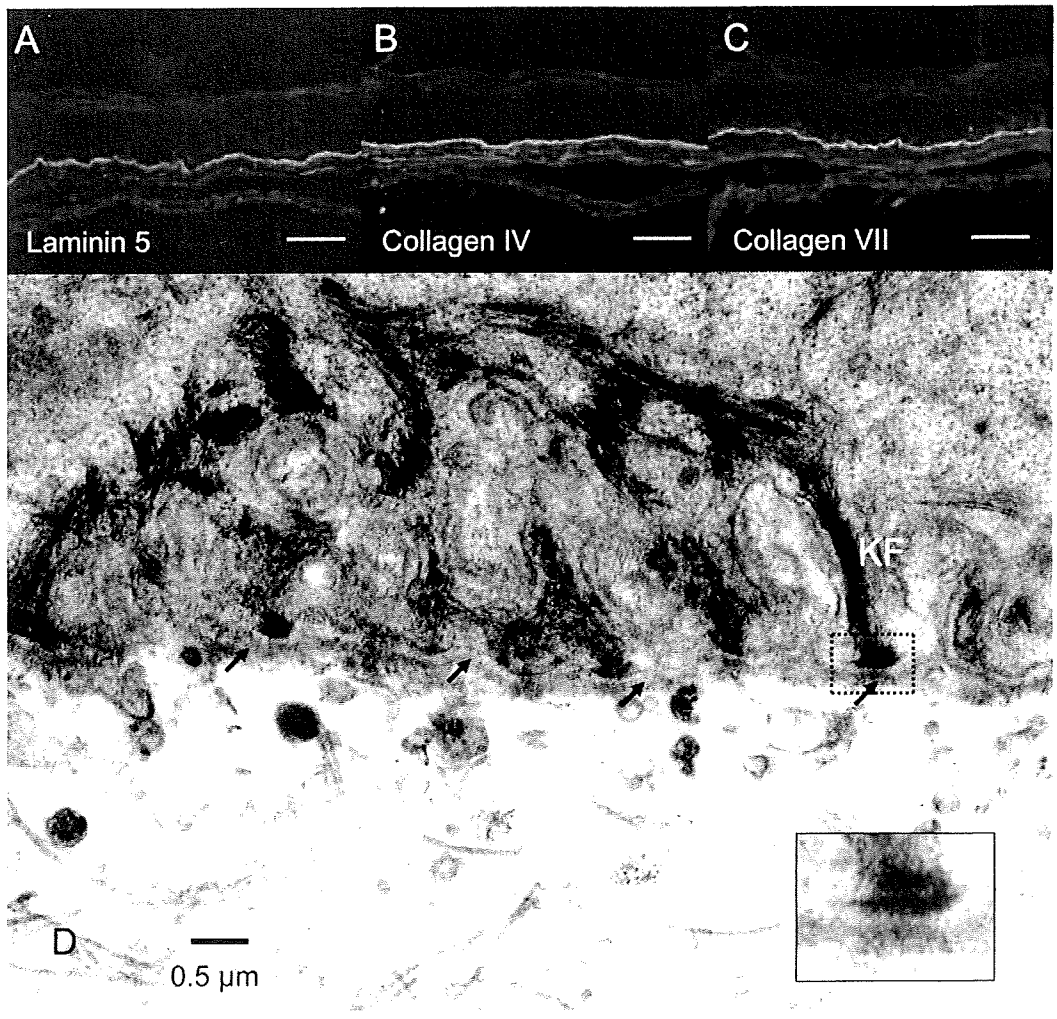

Fig. 4. Basement membrane development in living skin equivalents. On frozen sections of living skin equivalent samples, the expression of laminin 5 (A), type IV collagen (B), and type VII collagen (C) were determined by immunofluorescence staining with the respective monoclonal antibodies. Transmission electron microscopy revealed a continuous lamina densa (arrows in D) and well developed hemidesmosomes (inset in D). KF, keratin filaments. Bars are 50 μm in A, B, and C and 0.5 μm in D.

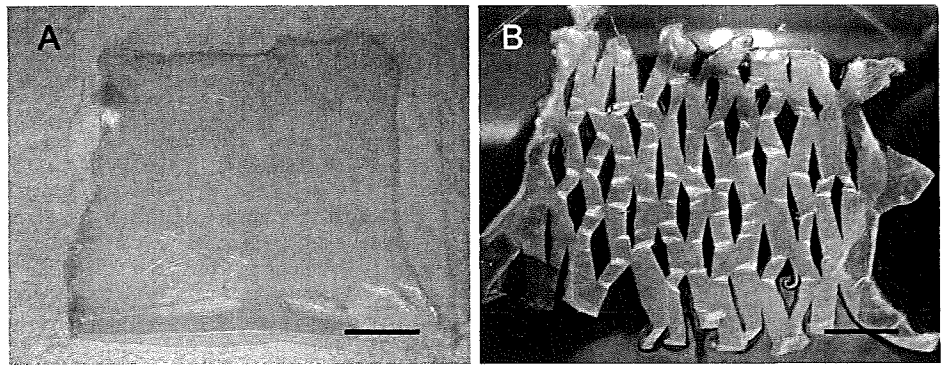

Fig. 5. A large living skin equivalent showed good mechanical properties. An amnion living skin equivalent (LSE) was made with an amnion of 4 × 4 cm. At day 7 after airlift, the LSE was lifted and made into a mesh-skin graft with a scalpel. The LSE was photographed before (A) and after (B) the mesh-skin graft processing. Bars are 1 cm.

E-cadherin and desmoglein 3 (Dsg 3) around each cell (Fig. 3C and D). We also noticed polarization of the epidermal cells, as shown by the distribution of integrin alpha 2 and integrin beta 4, which was restricted to the basal and lower suprabasal layer of the epidermis (Fig. 3E and F). The distribution of keratin 10 extended from the suprabasal layer to the stratum corneum (Fig. 3G), indicating the differentiated status of the keratinocytes. Keratin 14 was seen in the basal and suprabasal layers, indicating the proliferative status of the cells (Fig. 3H).

Considering BM development is important when investigating a cultivated LSE. IF staining revealed linear and compact deposition of the major BM proteins, laminin 5, and types IV and VII collagen at the epidermal–dermal junction (Fig. 4A–C). The development of the BM zone was further examined using transmission electron microscopy (TEM). A continuous lamina densa was formed along the plasma membrane of the keratinocytes, with many hemidesmosomes. The hemidesmosomes were well developed structurally, with inner and outer plaques clearly distinguished; keratin filaments were connected to the inner plaques (Fig. 4D).

3.3. Amnion LSEs showed good mechanical and handling properties

At day 7 after airlift, the large amnion LSE was ready for use, with a yellowish color to the cornified epidermis (Fig. 5A). The LSE was readily lifted from the culture insert and transferred to a culture dish with forceps, without separation of the epidermis and dermis or rupture of the dermal matrix. Furthermore, the amnion LSE was firm enough to tolerate scalpel cutting and could be stretched to prepare a mesh-skin graft (Fig. 5B).

3.4. Amnion LSE graft on nude mice was well vascularized and showed good morphology

Two weeks after transplantation, the grafts had survived on nude mice, with even surfaces and a pink coloration (Fig. 6A). The grafts were harvested and processed for H&E staining. The epidermis was well stratified, with columnar basal cells compactly aligned along the epidermal–dermal junction, round spinous cells and flat granular cells in the upper layers, and a thick stratum corneum on the surface. The amnion could still be distinguished by an acellular zone, which remained uninfiltrated by underlying mesenchymal cells. In the substratum, many small blood vessels were found up to the acellular zone (Fig. 6B).

4. Discussion

In this study, we confirmed that keratinocytes spread and proliferated well on the epithelial side of de-epithelialized amnions, and found that the stroma of amnions supported fibroblast adherence and infiltration. The LSE was constructed by seeding keratinocytes on fibroblast-infiltrated amnions and was investigated *in vitro* and *in vivo*.

Amnions can be de-epithelialized and preserved, with intact basal lamina remaining [34,35]. The exposed BM components of amnions enhance corneal epithelial cell adherence, proliferation, and migration [19]. In this study, we found that normal human

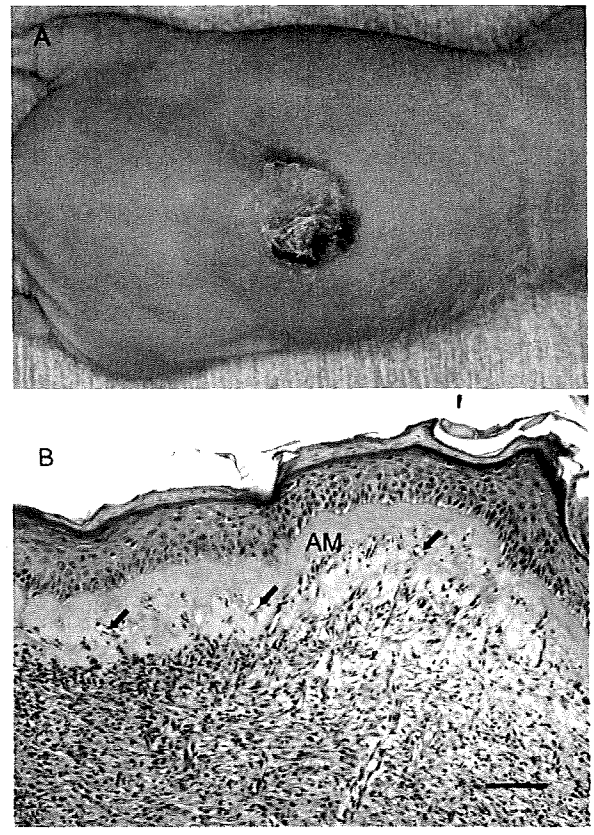

Fig. 6. Morphology of the living skin equivalent grafts. The living skin equivalents (LSEs) were grafted onto full-thickness wounds on the backs of nude mice. Two weeks later, the gross appearance of the grafts was photographed and the grafts were harvested and processed for H&E staining. A well stratified and differentiated epidermis was observed. Many small blood vessels were found in the substratum of the graft (arrows) up to near the thin acellular zone, which separated the epidermis and underlying substratum. AM, amnion. Bar is 50 μm.

keratinocytes attached and spread faster on de-epithelialized AM and that confluent cells were more compactly arranged than on type I collagen. Also, in a previous study, we showed that newly formed epidermis expanded faster on de-epithelialized amnions than on fibroblast-populated type I collagen gel [32]. Among the main BM components, type IV collagen has been shown to enhance human keratinocyte spread and growth [36], and laminin 5, a key component of the anchoring complex of the BM, is also essential for keratinocyte attachment, polarization, and migration [37–39].

When constructing a LSE, preexisting BM components on the dermal matrix contribute to improving the morphology of the epidermis and are necessary for the formation of hemidesmosomes and the development of a lamina densa [9,40,41]. Epithelial–mesenchymal interactions play important roles in controlling epidermal morphogenesis and homeostasis. The interaction between keratinocytes and the insoluble BM proteins contributes to the maintenance of tissue architecture and affects various biological processes, such as cell attachment, proliferation, differentiation, and migration [42,43]. On the de-epithelialized AM, the epidermis was well differentiated, stratified, and polarized, with columnar basal cells compactly aligned along the dermal–epidermal junction. These results indicated that the presence of certain BM components on de-epithelialized AM improved the homeostasis of the overlying epidermis.

The well developed basal lamina and hemidesmosomes in the amnion LSE guaranteed a stable association between the epidermis and the underlying tissues, which could explain why the epidermis was resistant to separation from the underlying connective tissue when the LSEs were harvested and manipulated for grafting.

Fibroblasts support epidermal morphogenesis and the deposition of BM components in preparing a LSE [44,45]. We constructed a LSE by seeding keratinocytes on de-epithelialized amnions; however, without coculturing fibroblasts in the stroma of the amnions, the resulting epidermis was thin and the basal cells were not well organized (data not shown). Because fibroblasts are known to support the growth of monolayer keratinocytes, we prepared fibroblasts in six-well plates to nourish the keratinocytes, which were seeded onto de-epithelialized amnions in culture inserts (set in six-well plates), and cultivated the keratinocytes at the air–liquid interface. However, the resulting epidermis of the LSEs was only two to three layers thick, and the cells were disorganized on the amnions (data not shown). It appears that fibroblasts being cultivated in the dermal matrix and the formation of a three-dimensional network are important for a well organized and differentiated epidermis in a LSE.

In the transplantation experiment, amnion LSEs were readily harvested from the culture inserts and transferred to full-thickness wounds on the backs of nude mice. The LSE grafts survived well on the nude mice and were well vascularized, as seen in the H&E-stained sections.

We also confirmed some other advantages in making the amnion LSE. First, we did not use any animal-derived type I collagen gel, which is conventionally employed in constructing the dermal matrix for a LSE [33]. Type I collagen is costly and may cause inflammatory reactions upon transplantation, and ethical issues may arise because of its animal origin [46]. Second, the procedure is simpler in making a fibroblast-infiltrated amnion than a fibroblast-populated collagen gel, which requires the mixing of several different ingredients while stirring on ice. Third, amnions as the matrix are more resistant to shear forces than collagen gel, which greatly facilitates the manipulation in removing the LSE from the culture insert and transferring it to a wound bed in transplantation.

In conclusion, the LSE with amnions as the dermal matrix demonstrated various advantages, such as a simple cultivating procedure, low cost, good mechanical and handling properties, and containing no animal products. Good epidermogenesis was seen *in vivo* and *in vitro*, suggesting that this LSE may be useful for clinical applications.

Acknowledgments

We thank Keiko Ozaki, Teruko Tsuda, and Eriko Tan for their technical assistance. This work was supported in part by grants from the Ministries of Education, Culture, Sports, Science and Technology, Japan, and in part by Health and Labor Sciences Research Grants (Research on Intractable Diseases) from the Ministry of Health, Labour and Welfare of Japan.

References

[1] Waymack P, Duff RG, Sabolinski M. The effect of a tissue engineered bilayered living skin analog, over meshed split-thickness autografts on the healing of excised burn wounds. The Apligraf Burn Study Group. Burns 2000;26:609–19.
[2] Falanga V, Margolis D, Alvarez O, Auletta M, Maggiacomo F, Altman M, et al. Rapid healing of venous ulcers and lack of clinical rejection with an allogeneic cultured human skin equivalent. Human Skin Equivalent Investigators Group. Arch Dermatol 1998;134:293–300.
[3] Kirsner RS. The use of Apligraf in acute wounds. J Dermatol 1998;25:805–11.
[4] Andriani F, Margulis A, Lin N, Griffey S, Garlick JA. Analysis of microenvironmental factors contributing to basement membrane assembly and normalized epidermal phenotype. J Invest Dermatol 2003;120:923–31.
[5] Jean J, Lapointe M, Soucy J, Pouliot R. Development of an in vitro psoriatic skin model by tissue engineering. J Dermatol Sci 2009;53:19–25.
[6] Wang X, Liu Y, Deng Z, Dong R, Liu Y, Hu S, et al. Inhibition of dermal fibrosis in self-assembled skin equivalents by undifferentiated keratinocytes. J Dermatol Sci 2009;53:103–11.
[7] Meana A, Iglesias J, Del Rio M, Larcher F, Madrigal B, Fresno MF, et al. Large surface of cultured human epithelium obtained on a dermal matrix based on live fibroblast-containing fibrin gels. Burns 1998;24:621–30.
[8] Llames SG, Del Rio M, Larcher F, Garcia E, Garcia M, Escamez MJ, et al. Human plasma as a dermal scaffold for the generation of a completely autologous bioengineered skin. Transplantation 2004;77:350–5.
[9] Medalie DA, Eming SA, Collins ME, Tompkins RG, Yarmush ML, Morgan JR. Differences in dermal analogs influence subsequent pigmentation, epidermal differentiation, basement membrane, and rete ridge formation of transplanted composite skin grafts. Transplantation 1997;64:454–65.
[10] Guerret S, Govignon E, Hartmann DJ, Ronfard V. Long-term remodeling of a bilayered living human skin equivalent (Apligraf) grafted onto nude mice: immunolocalization of human cells and characterization of extracellular matrix. Wound Repair Regen 2003;11:35–45.
[11] Ojeh NO, Frame JD, Navsaria HA. In vitro characterization of an artificial dermal scaffold. Tissue Eng 2001;7:457–72.
[12] Morykwas MJ, Thornton JW, Bartlett RH. Zeta potential of synthetic and biological skin substitutes: effects on initial adherence. Plast Reconstr Surg 1987;79:732–9.
[13] Ravishanker R, Bath AS, Roy R. "Amnion Bank"—the use of long term glycerol preserved amniotic membranes in the management of superficial and superficial partial thickness burns. Burns 2003;29:369–74.
[14] Gajiwala K, Gajiwala AL. Evaluation of lyophilised, gamma-irradiated amnion as a biological dressing. Cell Tissue Bank 2004;5:73–80.
[15] Quinby Jr WC, Hoover HC, Scheflan M, Walters PT, Slavin SA, Bondoc CC. Clinical trials of amniotic membranes in burn wound care. Plast Reconstr Surg 1982;70:711–7.
[16] Park M, Kim S, Kim IS, Son D. Healing of a porcine burn wound dressed with human and bovine amniotic membranes. Wound Repair Regen 2008;16:520–8.
[17] Mohammadi A, Johari HG. Amniotic membrane: a skin graft fixator convenient for both patient and surgeon. Burns 2008;34:1051–2.
[18] Oyama N, Bhogal BS, Carrington P, Gratian MJ, Black MM. Human placental amnion is a novel substrate for detecting autoantibodies in autoimmune bullous diseases by immunoblotting. Br J Dermatol 2003;148:939–44.
[19] Koizumi N, Fullwood NJ, Bairaktaris G, Inatomi T, Kinoshita S, Quantock AJ. Cultivation of corneal epithelial cells on intact and denuded human amniotic membrane. Invest Ophthalmol Vis Sci 2000;41:2506–13.
[20] Nakamura T, Endo K, Cooper LJ, Fullwood NJ, Tanifuji N, Tsuzuki M, et al. The successful culture and autologous transplantation of rabbit oral mucosal epithelial cells on amniotic membrane. Invest Ophthalmol Vis Sci 2003;44:106–16.
[21] Sakamoto T, Hirano K, Morishima Y, Masuyama K, Ishii Y, Nomura A, et al. Maintenance of the differentiated type II cell characteristics by culture on an acellular human amnion membrane. In Vitro Cell Dev Biol Anim 2001;37:471–9.
[22] Espana EM, He H, Kawakita T, Di Pascuale MA, Raju VK, Liu CY, et al. Human keratocytes cultured on amniotic membrane stroma preserve morphology and express keratocan. Invest Ophthalmol Vis Sci 2003;44:5136–41.

[23] Kumar TR, Shanmugasundaram N, Babu M. Biocompatible collagen scaffolds from a human amniotic membrane: physicochemical and in vitro culture characteristics. J Biomater Sci Polym Ed 2003;14:689–706.
[24] Kubo M, Sonoda Y, Muramatsu R, Usui M. Immunogenicity of human amniotic membrane in experimental xenotransplantation. Invest Ophthalmol Vis Sci 2001;42:1539–46.
[25] Solomon A, Wajngarten M, Alviano F, Anteby I, Elchalal U, Pe'er J, et al. Suppression of inflammatory and fibrotic responses in allergic inflammation by the amniotic membrane stromal matrix. Clin Exp Allergy 2005;35:941–8.
[26] Burman S, Tejwani S, Vemuganti GK, Gopinathan U, Sangwan VS. Ophthalmic applications of preserved human amniotic membrane: a review of current indications. Cell Tissue Bank 2004;5:161–75.
[27] von Versen-Hoynck F, Syring C, Bachmann S, Moller DE. The influence of different preservation and sterilisation steps on the histological properties of amnion allografts—light and scanning electron microscopic studies. Cell Tissue Bank 2004;5:45–56.
[28] Rejzek A, Weyer F, Eichberger R, Gebhart W. Physical changes of amniotic membranes through glycerolization for the use as an epidermal substitute. Light and electron microscopic studies. Cell Tissue Bank 2001;2:95–102.
[29] von Versen-Hoeynck F, Steinfeld AP, Becker J, Hermel M, Rath W, Hesselbarth U. Sterilization and preservation influence the biophysical properties of human amnion grafts. Biologicals 2008;36:248–55.
[30] Shirakata Y, Ueno H, Hanakawa Y, Kameda K, Yamasaki K, Tokumaru S, et al. TGF-beta is not involved in early phase growth inhibition of keratinocytes by 1alpha,25(OH)2vitamin D3. J Dermatol Sci 2004;36:41–50.
[31] Shirakata Y, Tokumaru S, Yamasaki K, Sayama K, Hashimoto K. So-called biological dressing effects of cultured epidermal sheets are mediated by the production of EGF family, TGF-beta and VEGF. J Dermatol Sci 2003;32:209–15.
[32] Yang L, Shirakata Y, Shudou M, Dai X, Tokumaru S, Hirakawa S, et al. New skin-equivalent model from de-epithelialized amnion membrane. Cell Tissue Res 2006;326:69–77.
[33] Yang L, Shirakata Y, Tamai K, Dai X, Hanakawa Y, Tokumaru S, et al. Microbubble-enhanced ultrasound for gene transfer into living skin equivalents. J Dermatol Sci 2005;40:105–14.
[34] Cooper LJ, Kinoshita S, German M, Koizumi N, Nakamura T, Fullwood NJ. An investigation into the composition of amniotic membrane used for ocular surface reconstruction. Cornea 2005;24:722–9.
[35] Nakamura T, Yoshitani M, Rigby H, Fullwood NJ, Ito W, Inatomi T, et al. Sterilized, freeze-dried amniotic membrane: a useful substrate for ocular surface reconstruction. Invest Ophthalmol Vis Sci 2004;45:93–9.
[36] Woodley DT, Wynn KC, O'Keefe EJ. Type IV collagen and fibronectin enhance human keratinocyte thymidine incorporation and spreading in the absence of soluble growth factors. J Invest Dermatol 1990;94:139–43.
[37] Nishiyama T, Amano S, Tsunenaga M, Kadoya K, Takeda A, Adachi E, et al. The importance of laminin 5 in the dermal-epidermal basement membrane. J Dermatol Sci 2000;24:S51–9.
[38] Frank DE, Carter WG. Laminin 5 deposition regulates keratinocyte polarization and persistent migration. J Cell Sci 2004;117:1351–63 [Epub 2004 Mar 1302].
[39] Kikkawa Y, Umeda M, Miyazaki K. Marked stimulation of cell adhesion and motility by ladsin, a laminin-like scatter factor. J Biochem (Tokyo) 1994;116:862–9.
[40] Kim SW, Park KC, Kim HJ, Cho KH, Chung JH, Kim KH, et al. Effects of collagen IV and laminin on the reconstruction of human oral mucosa. J Biomed Mater Res 2001;58:108–12.
[41] Ralston DR, Layton C, Dalley AJ, Boyce SG, Freedlander E, Mac Neil S. The requirement for basement membrane antigens in the production of human epidermal/dermal composites in vitro. Br J Dermatol 1999;140:605–15.
[42] Blomme EA, Weckmann MT, Capen CC, Rosol TJ. Influence of extracellular matrix macromolecules on normal human keratinocyte phenotype and parathyroid hormone-related protein secretion and expression in vitro. Exp Cell Res 1998;238:204–15.
[43] Kim JP, Chen JD, Wilke MS, Schall TJ, Woodley DT. Human keratinocyte migration on type IV collagen. Roles of heparin-binding site and alpha 2 beta 1 integrin. Lab Invest 1994;71:401–8.
[44] Erdag G, Sheridan RL. Fibroblasts improve performance of cultured composite skin substitutes on athymic mice. Burns 2004;30:322–8.
[45] El Ghalbzouri A, Ponec M. Diffusible factors released by fibroblasts support epidermal morphogenesis and deposition of basement membrane components. Wound Repair Regen 2004;12:359–67.
[46] Klein B, Schiffer R, Hafemann B, Klosterhalfen B, Zwadlo-Klarwasser G. Inflammatory response to a porcine membrane composed of fibrous collagen and elastin as dermal substitute. J Mater Sci Mater Med 2001;12:419–24.

The American Journal of Pathology, Vol. 175, No. 5, November 2009

DOI: 10.2353/ajpath.2009.090420

Vascular Biology, Atherosclerosis and Endothelium Biology

Nodal Lymphangiogenesis and Metastasis

Role of Tumor-Induced Lymphatic Vessel Activation in Extramammary Paget's Disease

Satoshi Hirakawa,*† Michael Detmar,‡ Dontscho Kerjaschki,§ Shogo Nagamatsu,* Keitaro Matsuo,¶ Atsushi Tanemura,‖ Nobuyuki Kamata,** Koichiro Higashikawa,** Hidenori Okazaki,* Kenji Kameda,†† Hisayo Nishida-Fukuda,* Hideki Mori,* Yasushi Hanakawa,* Koji Sayama,* Yuji Shirakata,* Mikiko Tohyama,* Sho Tokumaru,* Ichiro Katayama,‖ and Koji Hashimoto*

From the Departments of Dermatology and Bioscience,†† Integrated Center for Sciences, Ehime University Graduate School of Medicine, Ehime, Japan; the Department of Cell Growth and Tumor Regulation,† Ehime Proteo-Medicine, Research Center, Ehime University, Ehime, Japan; the Institute of Pharmaceutical Sciences,‡ Swiss Federal Institute of Technology, Eidgenössische Technische Hochschule Zurich, Zurich, Switzerland; the Clinical Institute of Pathology,§ Medical University Vienna, Vienna, Austria; the Division of Epidemiology and Prevention,¶ Aichi Cancer Center Research Institute, Nagoya, Japan; the Department of Dermatology,‖ Osaka University Graduate School of Medicine, Osaka, Japan; and the Department of Oral and Maxillofacial Surgery,** Division of Cervico-Gnathostomatology, Graduate School of Biomedical Sciences, Hiroshima University, Hiroshima, Japan*

Nodal lymphangiogenesis promotes distant lymph node (LN) metastasis in experimental cancer models. However, the role of nodal lymphangiogenesis in distant metastasis and in the overall survival of cancer patients remains unknown. Therefore, we investigated mechanisms that might facilitate regional and distant LN metastasis in extramammary Paget's disease (EMPD). We retrospectively analyzed the impact of tumor-induced lymphatic vessel activation on the survival of 116 patients, the largest cohort with EMPD studied to date. Nodal lymphangiogenesis was significantly increased in metastatic, compared with tumor-free, LNs ($P = 0.022$). Increased lymphatic invasion within regional LNs was significantly associated with distant metastasis in LN ($P = 0.047$) and organs ($P = 0.003$). Thus, invasion within regional LNs is a powerful indicator of systemic tumor spread and reduced patient survival in EMPD ($P = 0.0004$). Lymphatic vessels associated with tumors expressed stromal cell-derived factor-1 (SDF-1), whereas CXCR4 was expressed on invasive Paget cells undergoing epithelial-mesenchymal transition (EMT)-like process. A431 cells overexpressing Snail expressed increased levels of CXCR4 in the presence of transforming growth factor-β1. Haptotactic migration assays confirmed that Snail-induced EMT-like process promotes tumor cell motility via the CXCR4-SDF-1 axis. Sinusoidal lymphatic endothelial cells and macrophages expressed SDF-1 in subcapsular sinuses of lymph nodes before Paget cell arrival. Our findings reveal that EMT-related features likely promote lymphatic metastasis of EMPD by activating the CXCR4-SDF-1 axis. ***(Am J Pathol 2009, 175:2235–2248; DOI: 10.2353/ajpath.2009.090420)***

The metastatic spread of cancer cells from a primary site generally occurs in sentinel lymph nodes (LNs). Thus, the presence and extent of LN metastasis determines staging and prognosis in most human malignancies and often guides therapeutic decisions.[1] Although surgical resection of primary tumors and their regional LN metastases can cure several types of cancer, distant LN and organ metastases represent a significant therapeutic concern due to the absence of effective antimetastatic therapies.

Supported by a Grant-in-Aid for Scientific Research on Priority Areas (MEXT18013037 and MEXT20013032; to S.H.), a Grant-in-Aid for Scientific Research (C20592099; to H.M.), a Grant-in-Aid for Young Scientists (B18791323; to S.N.), the Nakajima Foundation (to S.H.), the Kanae Foundation for the Promotion of Medical Science (to S.H.), and Lydia O'Leary Memorial Foundation (to S.N.).

Accepted for publication July 28, 2009.

Address reprint requests to Satoshi Hirakawa, M.D., Ph.D., Department of Dermatology, Ehime University Graduate School of Medicine, Shitsukawa, Toon, Ehime 791-0295, Japan. E-mail: satoshi2@m.ehime-u.ac.jp.

The mechanisms of tumor cell metastasis to regional and distant LNs have remained unclear, mainly due to the absence of lymphatic-specific markers and lack of insight into the molecular mechanisms mediating tumor cell entry and persistence within the lymphatic system.

Recent studies have identified novel lymphatic-specific markers,[2,3] including the mucin-type glycoprotein podoplanin,[4] the lymphatic vascular endothelial cell hyaluronan receptor-1 (LYVE-1)[5] and the homeobox transcription factor Prox1.[6–8] Moreover, several lymphangiogenic growth factors have also been identified. Among these, vascular endothelial growth factor (VEGF)-C and VEGF-D activate VEGF receptor-3 (VEGFR-3) that is predominantly expressed by lymphatic endothelial cells (LECs).[9,10] More recently, VEGFR-3 has been shown to be expressed on tumor-associated blood vascular endothelial cells.[11] The angiogenesis factor VEGF-A also promotes lymphangiogenesis in the skin.[12–14] Importantly, VEGF-C, VEGF-D, or VEGF-A overexpression in experimental tumor models induces lymphatic vessel growth associated with primary tumors, leading to enhanced tumor metastasis to regional LNs.[15–18] Moreover, a blockade of VEGFR-3 signaling inhibits tumor lymphangiogenesis and LN metastasis in rodent models of tumor metastasis.[17,19]

We recently found that targeted VEGF-A or VEGF-C overexpression in the skin of a multistep chemically induced model of skin carcinogenesis promotes the lymphangiogenesis of primary tumors, which increases tumor metastasis to regional LNs and beyond.[18,20] More importantly, metastatic tumors that overexpress VEGF-A or VEGF-C also induced new lymphatic vessel growth within the regional LNs, probably contributing to enhanced distant LN metastasis. Thus, primary tumors in the skin induced LN lymphangiogenesis even before they metastasized, thereby preparing the lymphvascular niche, a tumor-conditioned microenvironment that serves as a future metastatic site within the regional LNs.[18,20,21]

Recent studies have shown that stromal cell-derived factor (SDF)-1, a ligand for the chemokine receptor CXCR4, is required for the formation of vascular niches that maintain hematopoietic stem cells in murine bone marrow.[22–24] Furthermore, CXCR4 is induced in several types of invasive cancers. In fact, several clinico-pathological studies have found that increased CXCR4 levels are associated with the survival of cancer cells, increased regional LN metastasis and/or reduced patient survival,[23,25,26] and vascular niches comprising tumor-associated blood vessel capillaries were found to serve as therapeutic targets in an experimental brain tumor model in mice.[27] However, the mechanisms that induce CXCR4 in invasive tumor cells remain unknown, and it has remained unclear whether the CXCR4-SDF-1 axis plays a significant role in the creation of the tumor-associated lymphvascular niche.

Increasing evidence indicates that tumor lymphangiogenesis arises in different types of human cancers, and that tumor-associated lymphatic vessel expansion is associated with enhanced rates of sentinel LN metastasis and reduced patient survival.[28–30] However, the mechanisms of tumor lymphangiogenesis and its relative importance to cancer metastasis and the survival of patients with different types of cancer have remained controversial. Therefore, the function(s) of tumor-associated lymphatic vessels need to be clarified so that interactions between tumor-associated LECs and invasive tumor cells within primary sites and the subsequent formation of LN metastasis can be understood in more detail.

Extramammary Paget's disease (EMPD) is a cutaneous adenocarcinoma that is characterized by the presence of vacuolated Paget cells.[31] The condition usually develops in genital and/or axillary skin and appears as an erythematous plaque at the early stages that is characterized by slow intraepidermal growth. During tumor progression, EMPD can develop nodules and ulcerations associated with local tissue invasion. Subsequently, tumors metastasize to regional LNs and distant organs, leading to a poor outcome.[32] Although these clinical features indicate that EMPD progression is associated with tumor lymphangiogenesis and angiogenesis, the occurrence and the pathogenetic role of vascular activation in EMPD have not been studied. Moreover, little is understood about the mechanisms through which Paget cells acquire the invasive phenotype that spreads to LNs and beyond.

The epithelial-mesenchymal transition (EMT), which plays a key role in promoting embryonic development, induces the striking transformation of epithelial cells to adopt the features of mesenchymal cells such as the expression of N-cadherin and loss of E-cadherin.[23,33,34] Recent studies have further proposed that cancer cells can acquire EMT-like phenotypes such as loss of cell polarity, loss of cell-cell adhesion, and/or loss of keratin expression and considerable expression of vimentin during tumor progression.[35,36] Among the molecular regulators of EMT-like processes in the tumor microenvironment, the transcription factor Snail initiates the down-regulation of E-cadherin expression in several tumor cells of epithelial origin, enabling these cells to detach from the tumor mass and to invade the surrounding stroma toward tumor-associated blood vessels to metastasize to distant organs.[37] The pleiotropic cytokine transforming growth factor (TGF)-β1 promotes EMT[38] but whether EMT-like behavior by tumor cells enhances their invasion of lymphatic vessels in primary sites remains obscure.

The present study investigates tumor angiogenesis, lymphangiogenesis, lymphatic invasion, and EMT-like phenotypes in 116 patients with EMPD, representing the largest cohort of this type analyzed in a single study. We investigated whether nodal lymphangiogenesis and/or lymphatic invasion within regional LNs promotes distant LN metastasis and examined the molecular mechanisms promoting lymphatic cancer spread in EMPD. Overall, we identified lymphatic invasion of regional LNs as a novel, significant prognostic indicator of metastasis and survival of patients with EMPD. Moreover, we found that invasive Paget cells undergoing EMT-like process express CXCR4, whereas its ligand SDF-1 is produced by tumor-associated lymphatic vessels and lymphatic sinuses of draining lymph nodes. Thus, the SDF1 axis plays an important role in mediating EMPD LN metastasis, and

CXCR4 expression by Paget cells predicts tumor metastasis and patient survival.

Materials and Methods

Patient Population

Patients with EMPD in the groin area were retrospectively identified through a review of survival data from the Graduate Schools of Medicine at Ehime and Osaka Universities. Surgical samples from primary skin tumors were collected from 116 patients and tissue samples of regional LNs were obtained from 45 of them. H&E staining of primary tumors in the skin identified carcinoma *in situ* (CIS) in 73 patients and invasive growth of primary tumors in the dermis of 43 of them. Regional LN metastasis was confirmed at the time of diagnosis in 20 of these patients and 23 had none. We also obtained representative sections from 17 patients with Bowen's disease, 42 patients with malignant melanoma *in situ*, and 15 normal skin samples from the surgical margin. This retrospective study was approved by the institutional review boards of the Graduate Schools of Medicine at Ehime and Osaka Universities.

Classification and Staging

Table 1 shows the clinical and pathological features used to diagnose EMPD. N-factors categorized no evident metastasis as N0, unilateral regional LN metastasis as N1, or bilateral regional LN metastasis as N2. We specifically categorized M-factors as no distant metastasis evident (M0), metastasis in distant LN(s) beyond regional LN(s), or metastasis in visceral organs (lung, liver, bone). Distant LN and organ metastases were detected by computer-assisted tomography, ultrasound examination, or skeletal scintigraphy. The Tumor Necrosis Metastasis classification for EMPD was designed and standardized by the Japanese Skin Cancer Society.[39]

Immunostaining

Primary tumors or LNs were fixed in buffered formalin, or embedded in OCT compound (Sakura Finetek, Torrance, CA) and snap-frozen. Paraffin (5 μm) or cryostat sections were immunostained as previously described,[18,20] using the primary antibodies shown in Table 2. The respective secondary antibodies were labeled with Alexa Fluor 488 or 594 (Molecular Probes, Eugene, OR). Antigens were usually retrieved in paraffin sections by incubation with citrate buffer (pH 6.0 for 30 minutes at 95°C) before immunostaining. Nuclei were counterstained with 4′,6′-diamidino-2-phenylindole (DAPI) (Molecular Probes). Sections were also immunohistochemically stained using a 3-amino-9-ethylcabazole peroxidase substrate kit (Vector Laboratories, Burlingame, CA). Respective control IgG was stained as a specificity control. Sections were examined, and digital images were captured using a confocal laser scanning microscope LSM510 (Carl Zeiss, Jena, Germany) or A1 (Nikon, Tokyo, Japan).

Table 1. Clinical and Pathological Characteristics of Patients with EMPD

Category	Nonmetastatic	Metastatic
No. of patients	96	20
Male	66	19
Female	30	1
Age at diagnosis (yr)		
Mean	71.3	71.1
Range	45–92	44–82
Stage		
IA, T1N0M0	72	0
IB, T2N0M0	21	0
II, T3N0M0	2	0
III, T4N0M0, anyTN1M0	1	8
IV, any TN2M0, any T any NMLN, any T any NMVO	0	12
T-factor		
T1, Carcinoma *in situ*	72	0
T2, Microinvasive	21	2
T3, Invasive without vascular invasion	2	4
T4, Invasive with vascular invasion	1	14
N-factor		
N0, Metastasis undetectable	96	0
N1, Unilateral regional LN metastasis	0	11
N2, Bilateral regional LN metastasis	0	9
M-factor		
M0, Distant metastasis undetectable	100	0
MLN, Metastasis in distant LN beyond regional LN	0	15
MVO, Metastasis in visceral organs (lung, liver, bone)	0	14

Units, except for age, are shown as numbers at time of diagnosis.

Computer-Assisted Morphometric Vessel Analyses

Representative sections obtained from 116 patients with primary EMPD, 17 with Bowen's disease, 42 with malignant melanoma *in situ*, and from 15 samples of normal skin were double-stained by differential immunofluorescence for podoplanin and von Willebrand factor, and then analyzed using a LSM 510 microscope (Carl Zeiss). Computer-assisted morphometric analyses of blood and lymphatic vessels on captured images proceeded using IP-LAB software (Scanalytics, Billerica, MA) as described previously.[18,20] Data are displayed as box and whisker plots.

Culture of LECs and Enzyme-Linked Immunosorbent Assays

Primary human dermal LECs were isolated from neonatal foreskins as described previously.[40] LECs (1×10^4) were seeded onto triplicate fibronectin-coated culture dishes

Table 2. Antibodies Used for Immunofluorescence and Immunohistochemistry

Antibody	Staining for	Source	Type
NZ-1 for podoplanin	Lymphatics	Y Kato	Rat monoclonal, IgG_{2a}
D2–40 for podoplanin	Lymphatics	Nichirei Biosciences	Mouse monoclonal, IgG_1
Prox1	Lymphatics	RELIATEC	Rabbit polyclonal
LYVE-1	Lymphatics	RELIATEC	Rabbit polyclonal
VEGFR-3	Lymphatics	R&D Systems	Goat polyclonal
Neuropilin-2	Lymphatics	R&D Systems	Goat polyclonal
von Willebrand factor	Panvascular	Dako	Rabbit polyclonal
MIB-1 for Ki-67	Proliferating cells	Dako	Mouse monoclonal, IgG_1
Cytokeratin 7	Paget cells	Dako	Mouse monoclonal, IgG_1
VEGF-A	Paget cells, immune cells	Thermo Fisher Scientific Inc.	Rabbit polyclonal
VEGF-C	Paget cells	Immuno-Biological Laboratories	Rabbit polyclonal
E-cadherin	Paget cells	Epitomics	Rabbit polyclonal
N-cadherin	Paget cells (EMT-like)	Upstate	Mouse monoclonal, IgG_1
Vimentin	Paget cells (EMT-like)	Dako	Mouse monoclonal, IgG_1
CXCR4	Invasive Paget cells	R&D Systems	Mouse monoclonal, IgG_{2a}
SDF-1	Tumor-associated lymphatics	R&D Systems	Mouse monoclonal, IgG_1
KP1 for CD68	Macrophages	Dako	Mouse monoclonal, IgG_1
HAM56	Macrophages	Dako	Mouse monoclonal, IgM

and propagated in endothelial cell growth medium[40] containing 0.5% fetal bovine serum (Invitrogen, Grand Island, NY). Conditioned media were collected at days 1, 3, or 5. Human SDF-1α or CCL21 levels were subsequently measured using enzyme-linked immunosorbent assays (ELISAs; Quantikine M; R&D Systems, Minneapolis, MN). Data were normalized to cell number at each time point.

Flow Cytometry and Haptotactic Cell Migration Assays

Recombinant human TGF-β1, human SDF-1α and anti-human CXCR4 monoclonal antibody 12G5 were purchased from R&D Systems. A431 cells stably transfected with mouse Snail or control pcDNA 3.1 (Invitrogen, Carlsbad, CA) vector were incubated with or without 10 ng/ml of recombinant human TGF-β1.[41] Single cell suspensions were prepared using cell dissociation buffer (Invitrogen). These cells were stained with the biotinylated anti-CXCR4 antibody 12G5, and then positively and negatively labeled with streptavidin-conjugated Alexa Fluor 488 (BD Biosciences Pharmingen) and propidium iodide, respectively. Stained cells (>10,000 cells/sample) were analyzed by flow cytometry using a FACScan and a FACSCalibur (BD Biosciences) and analyzed by FlowJo software (Tree Star, San Carlos, CA). For migration assays, cells were seeded in serum-free Dulbecco's modified Eagle's medium containing 0.2% delipidized bovine serum albumin into the upper chambers of 24-well FluoroBlok inserts (BD Biosciences) in the presence of human CXCR4-neutralizing monoclonal antibody 12G5 (10 μg/ml), or corresponding control IgG, and incubated for 3 hours at 37°C in the presence of SDF-1α in the bottom chambers. Cells on the undersides of inserts were stained with DAPI (Molecular Probes), and migrated cells were counted by computer-assisted image analysis of three random ×10 fields per well. Three independent experiments were performed for each assay.

Statistical Analyses

Across-group comparisons were performed by one-way analysis of variance when appropriate, followed by *t*-tests for pairwise comparisons. *P* values were adjusted using Bonferroni's method. Trends were analyzed by linear regression adjusted for age and gender. Overall survival after the date of surgery was defined as the primary endpoint. The Kaplan-Meier product limit method was applied and comparisons according to markers were examined using the log-rank test. We defined $P < 0.05$ as statistically significant.

Results

Increased Tumor Lymphangiogenesis and Angiogenesis in EMPD

The macroscopic appearance of EMPD is characterized by a red patch, usually in the groin region, indicating a high level of vascularization (Figure 1A). Routine H&E stain showed a few number of small vessels in normal skin (Figure 1B). In contrast, histology in EMPD revealed a hyperplastic epidermis and prominent enlargement of numerous vessels within the dermis (Figure 1C) as compared with normal skin (Figure 1B). The majority of epidermal cells are composed of round Paget cells with clear and abundant cytoplasm with hyperchromatic nuclei (Figure 1C, inset). Within a hyperplastic epidermis, tumors occasionally invaded the vasculature during tumor progression (Figure 1D), indicating the metastatic potential of invasive Paget cells.

Because VEGF-A and VEGF-C have been identified as tumor lymphangiogenesis factors in experimental mouse models, we investigated their expression in EMPD by immunohistochemistry. Levels of VEGF-A were high in both Paget cells and in inflammatory cells in various grades of primary tumors (Figure 1G) but not in normal skin (Figure

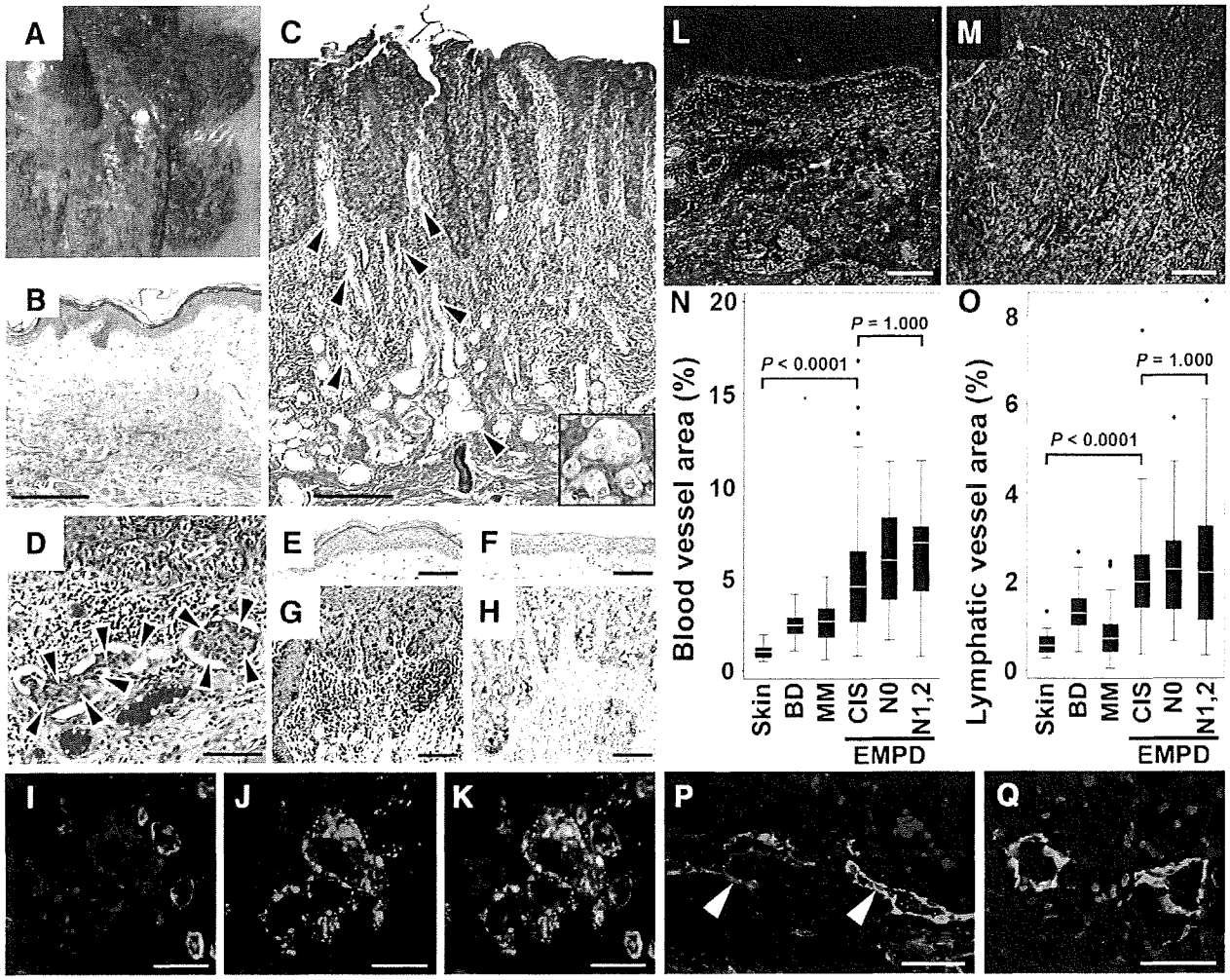

Figure 1. Tumor lymphangiogenesis and angiogenesis in EMPD. **A:** Macroscopic appearance of EMPD. Red plaque over groin of 64-year-old male patient. **B** and **C:** In contrast to routine H&E staining of normal skin with a small number of vessels (**B**), H&E staining in EMPD reveals that numerous vessels are significantly enlarged and that these vessels actively penetrate for the hyperplastic epidermis (**C, arrowheads**). Paget cells in the epidermis show clear and abundant cytoplasm with hyperchromatic nuclei (**C, inset**). **D:** Vascular invasion by Paget cells detected by routine H&E staining (**arrowheads** indicate tumor invasion within two vessels in primary site). **E** and **G:** Abundant VEGF-A expression (red) by Paget cells in epidermis and by inflammatory cells in dermis (**G**), whereas normal skin does not specifically express VEGF-A (**E**). **I–K:** Subpopulation of immune cells producing VEGF-A (**I**, red) identified as CD68-positive macrophages (**J**, green; **K**, yellow). **F** and **H:** VEGF-C is exclusively produced by Paget cells (**H**) but not by normal skin (**F**). **L** and **M:** Double-immunofluorescence staining for anti-von Willebrand factor antibody (red) shows major expansion of blood vasculature in CIS of EMPD (**M**) compared with normal skin (**L**). Tumor lymphangiogenesis detected by staining for podoplanin (green) is also prominent in tumor-associated tissue (**M**). **N:** Computer-assisted morphometric analyses show enhanced tumor angiogenesis in EMPD compared with normal skin, Bowen's disease (BD), or malignant melanoma *in situ* (MM), indicating powerful angiogenic potency of EMPD. **O:** Relative LVAs are similar between metastatic and nonmetastatic EMPD. Tumor lymphangiogenesis was significantly induced at early stages of EMPD, indicating that some factor(s) other than lymphatic vessel proliferation affects the prognoses of patients with advanced EMPD. Data are expressed as means ± SD and are shown as box and whisker plots. **P:** Tumor-associated podoplanin-positive lymphatic vessels (green) are obviously stained for Ki-67 (red), indicating active lymphatic proliferation (**arrowheads**). These cells also expressed Prox1 (**Q**, red). Scale bars = 200 (**B** and **C**), 100 (**D–H**, **L**, and **M**), 10 (**I–K**) and 50 (**P** and **Q**) μm. MM, malignant melanoma *in situ*; N0, no regional LN metastasis; N1, unilateral inguinal LN metastasis; N2, bilateral inguinal LN metastasis.

1E). Double-immunofluorescence staining for VEGF-A and CD68 revealed that a subpopulation of immune cells producing VEGF-A in fact consisted of macrophages (Figure 1, I–K). VEGF-C was exclusively expressed in Paget cells within the epidermis (Figure 1H) and was undetectable in normal skin (Figure 1F). These results suggest that Paget cells induce both tumor lymphangiogenesis and angiogenesis via the secretion of VEGF-A and VEGF-C.

We then investigated the presence of tumor-associated lymphatic and blood vessels, using specific antibodies against podoplanin for lymphatic vessels,[42,43] and against von Willebrand factor for blood vessels. Differential immunofluorescence analyses revealed lymphatic and blood vessel formation at the early stage of CIS (Figure 1M), as compared with normal skin obtained from surgical margins (Figure 1L). Tumor lymphangiogenesis and angiogenesis were increased throughout the successive stages of EMPD tumor progression, as compared with normal skin. Computer-assisted morphometric analyses confirmed that relative tissue areas occupied by lymphatic vessels that were podoplanin-positive and by blood vessels that were positive for von Willebrand factor were increased in the peritumoral areas of CIS, as compared with normal skin (Figure 1, M and N; $P < 0.0001$, respectively). We then compared neovascularization in EMPD with other skin tumors such as Bo-

wen's disease or malignant melanoma *in situ* that histologically assume a pagetoid pattern within the epidermis (Figure 1, N and O). Tumor-associated angiogenesis and lymphangiogenesis were most obviously increased in EMPD, as compared with all other types of skin tumors ($P < 0.05$), indicating that EMPD is the most highly vascularized type of skin tumor. Levels of tumor angiogenesis and lymphangiogenesis in CIS were comparable with those in invasive EMPD in the absence (N0) or presence (N1,2) of regional LN metastases (Figure 1, M and N).

Differential immunofluorescence analysis of primary EMPD tumors for the proliferation marker Ki-67 and podoplanin revealed proliferating LECs in the peritumoral area, indicating active tumor lymphangiogenesis (Figure 1P). All podoplanin-positive vessels also expressed the lymphatic-specific transcription factor Prox1, confirming their lymphatic identity (Figure 1Q).

Tumor-Associated LECs Attract Aggressive Paget Cells via the CXCR4-SDF-1 Axis

Although the assessment of tumor-associated lymphatic vessel growth did not significantly contribute to estimating an increased frequency of regional LN metastasis in EMPD, we postulated that tumor-induced lymphatic vessels are functionally distinct from normal lymphatic vessels in the skin. In fact, a subpopulation of podoplanin and LYVE-1-positive, tumor-associated lymphatic vessels expressed large amounts of VEGFR-3 (Figure 2, A–C and D–F, arrows) whereas other lymphatic vessels did not, according to immunofluorescence staining (Figure 2, A–C and D–F, arrowheads). Furthermore, neuropilin-2 was highly induced in a subpopulation of podoplanin-positive tumor-associated LECs (Figure 2I, arrow). Therefore, these results suggest that tumor-associated LECs are functionally activated in EMPD and indicate that tumor-induced lymphatic vessels might positively mediate tumor cell invasion toward those lymphatic vessels and metastasis to regional LNs.

To define the potential role of specific chemokine-chemokine receptor interactions in promoting contact between Paget cells and LECs, we investigated whether SDF-1, a specific ligand for CXCR4, is expressed by lymphatic vessels associated with primary skin tumors. Double-immunofluorescence staining revealed that tumor-associated LYVE-1-positive lymphatic vessels were positive for SDF-1, whereas lymphatic vessels in normal skin were not (Figure 2, J–O). Furthermore, ELISAs showed that cultured LECs expressed marked levels of SDF-1, whereas LECs constitutively expressed CCL21, a known lymphoid tissue chemokine, in conditioned media (Figure 2P), indicating that SDF-1 may be secreted by LECs toward CXCR4-expressing cells.

To further elucidate the role of CXCR4 in promoting LN metastasis in EMPD, immunofluorescence staining revealed that highly invasive Paget cells indeed expressed CXCR4 (Figure 2Q). In contrast, Paget cells in CIS did not express detectable levels of CXCR4 (Figure 2R). Kaplan-Meier analysis revealed that the expression of CXCR4 on Paget cells represented a significant prognostic factor for reduced overall patient survival ($P < 0.0001$; Figure 2S). Taken together, these results suggest that tumor-associated LECs can chemoattract CXCR4-positive Paget cells toward lymphatic vessels within primary sites, and might play a crucial role in promoting LN metastasis, leading to a patient poor outcome.

EMT-Like Phenotypes Are Novel Prognostic Parameters for Reduced Survival in EMPD

To further characterize Paget cell motility toward lymphatic vessels within the primary sites, we initially investigated whether EMT-like process plays a significant role in promoting stromal invasion in EMPD. Immunofluorescence staining revealed that Paget cells in CIS do not express large amounts of E-cadherin on the cell membrane, in particular at the tumor-stroma interface, unlike normal epidermal keratinocytes (Figure 3, A, B, D, and E). The expression of E-cadherin was further altered in invasive Paget cells (Figure 3, C and F), and cytoplasmic E-cadherin expression was detectable by the early stages of tumor progression in a subpopulation of patients with a poor outcome (Figure 3F, arrowheads). Therefore, we calculated the overall survival of patients with or without detectable cytoplasmic E-cadherin expression using Kaplan-Meier analysis. The results showed that the expression of cytoplasmic E-cadherin was a significant prognostic factor for reduced overall survival in EMPD ($P = 0.0068$; Figure 3J).

Paget cells did not express N-cadherin and/or vimentin (mesenchymal markers) at the early stages of CIS (Figure 3, E and H) like normal epidermal keratinocytes (Figure 3, D and G) but did so in invasive EMPD (Figure 3, F and I). Kaplan-Meier analyses revealed that N-cadherin or vimentin expression in EMPD significantly correlated with reduced overall survival ($P < 0.0001$; Figure 3J), indicating that EMT-like process plays a key role in promoting tumor invasion within the primary sites.

EMT-Like Process Promotes Enhanced Chemotaxis to SDF-1 by Inducing CXCR4 in A431 Cells

Double-immunofluorescence staining showed that invasive Paget cells located at the edges of tumors expressed both N-cadherin and CXCR4 (Figure 4, A–C), indicating that EMT-related process in Paget cells might induce CXCR4 that enables invasive tumor cells to migrate toward tumor-associated SDF-1-secreting lymphatic vessels. To determine whether EMT-associated pathway increases CXCR4 expression on the surface of cancer cells, we investigated A431 cells that were stably transfected with Snail, a key transcription factor that induces EMT-like phenotypes in tumor cells. The expression of CXCR4 was considerably increased on the surface of transfected cells compared with mock-transfected A431 cells (Geo Mean: mock A431, 7.4%; Snail A431, 15.1%; Figure 4D). In addition, TGF-β1 further enhanced CXCR4 on Snail- but not on mock-transfected A431 cells (Geo Mean: mock A431, 9.5%; Snail

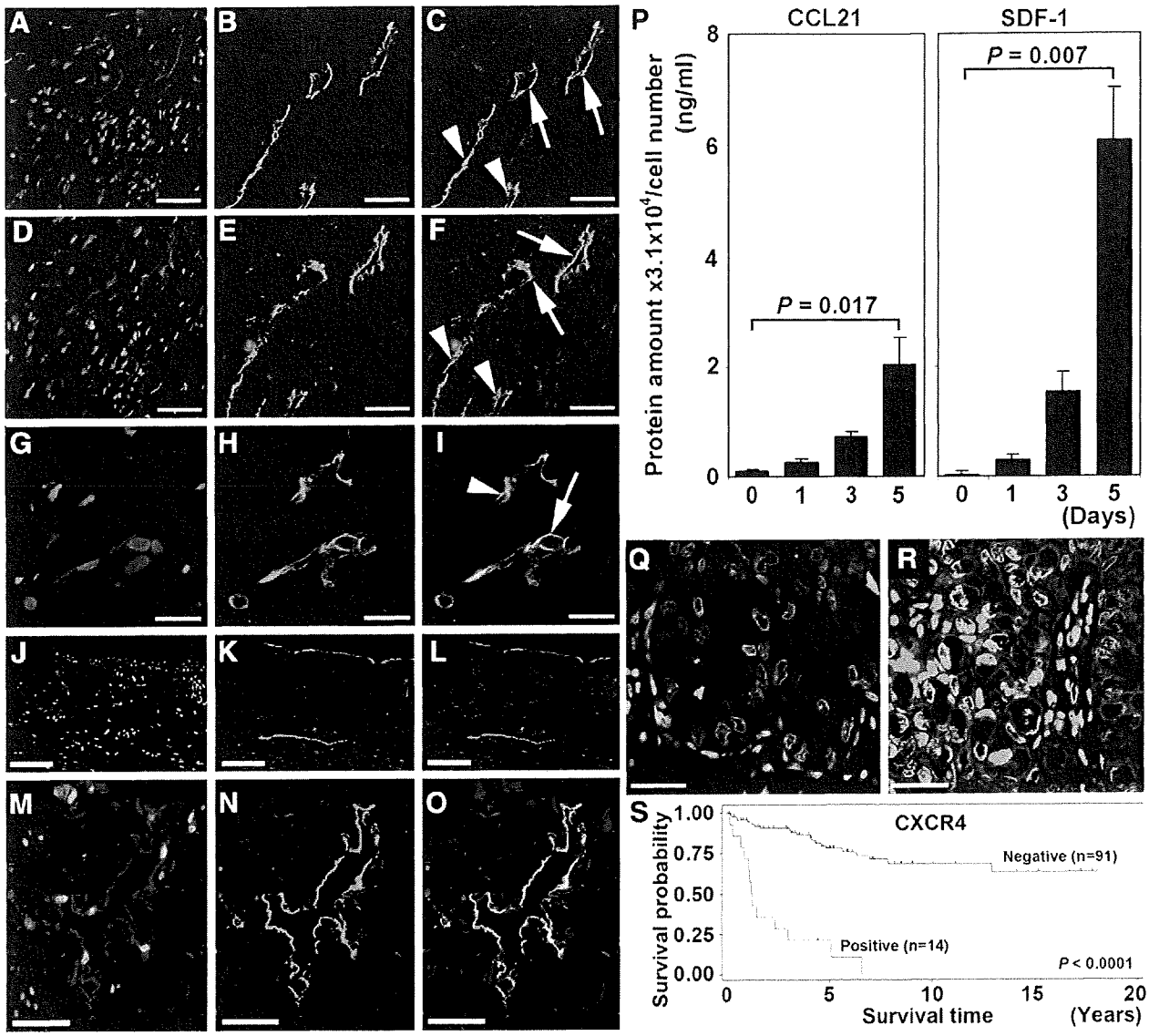

Figure 2. Functional activation of tumor-associated LECs and invasive Paget cells. The CXCR4-SDF-1 axis mediates Paget cell-LEC interactions within primary lesions of EMPD. **A–C:** VEGFR-3 (**A**, red) is significantly up-regulated in subpopulation of tumor-associated podoplanin-positive lymphatic vessels (**B**, green; **C**, **arrows**), indicating activation of lymphatic vessels in tumor microenvironment. Some lymphatic vessels do not express VEGFR-3 (**C**, **arrowheads**). **D–F:** Double immunofluorescence stains for LYVE-1 (**E**, green) and VEGFR-3 (**D**, red) using serial sections further confirmed that the activated lymphatic vessels (**F**, **arrows**) induce VEGFR-3 (**F**, yellow, **arrows**), whereas the other lymphatic vessels do not express VEGFR-3 (**F**, **arrowheads**). **G–I:** Neuropilin-2 (**G**, red) is prominently induced in subpopulation of tumor-associated podoplanin-positive LECs (**H**, green; **I**, yellow, **arrow**), whereas adjacent LECs reveal lower levels of neuropilin-2 within the primary site (**I**, green, **arrowhead**). **J–O: J–L** show normal skin. LYVE-1-positive lymphatic vessels (**K**, green) failed to express SDF-1, a specific ligand for CXCR4 (**J**, red), showing no merged color in panel **L**. Panels **M–O** demonstrate tumor microenvironment within the primary site. Tumor-associated LYVE-1-positive lymphatic vessels (**N**, green) express high levels of SDF-1 (**M**, red; **O**, yellow). **P:** Cultured LECs expressed CCL21 in a time-dependent pattern. Marked induction of SDF-1 was observed in conditioned media, as determined by ELISA. Data are expressed as means ± SD. **Q** and **R:** Immunofluorescence staining shows absence of CXCR4 expression in CISs (**Q**). In contrast, invasive Paget cells in advanced EMPD express membrane-specific CXCR4 (**R**, red). Nuclei are stained blue (DAPI stain). Scale bars = 50 (**A–F**), 10 (**G–I**), 100 (**J–O**), and 30 (**Q** and **R**) μm. **S:** Kaplan-Meier analysis of overall survival in EMPD shows that CXCR4 expressed by Paget cells is significantly associated with poor survival in EMPD.

A431, 36.6%; Figure 4E), indicating that EMT-like process promotes CXCR4 expression in A431, a vulval epidermoid tumor cell line, particularly in the presence of TGF-β1. Haptotactic migration assays further revealed enhanced chemotaxis toward SDF-1 in the lower chamber by TGF-β1-treated Snail-transfected A431 cells, compared with mock-transfected A431 cells in the upper chamber. In contrast, neutralization of CXCR4 on A431 cells significantly inhibited the enhanced chemotaxis toward SDF-1 (Figure 4F). Therefore, the CXCR4-SDF-1 axis plays a key role in promoting A431 cell motility undergoing EMT-like processes.

Lymphatic Invasion within the Primary Sites Indicates Expansion of Regional LN Metastases

On the basis of the findings with regard to the CXCR4-SDF-1 axis, we next evaluated 42 samples from patients

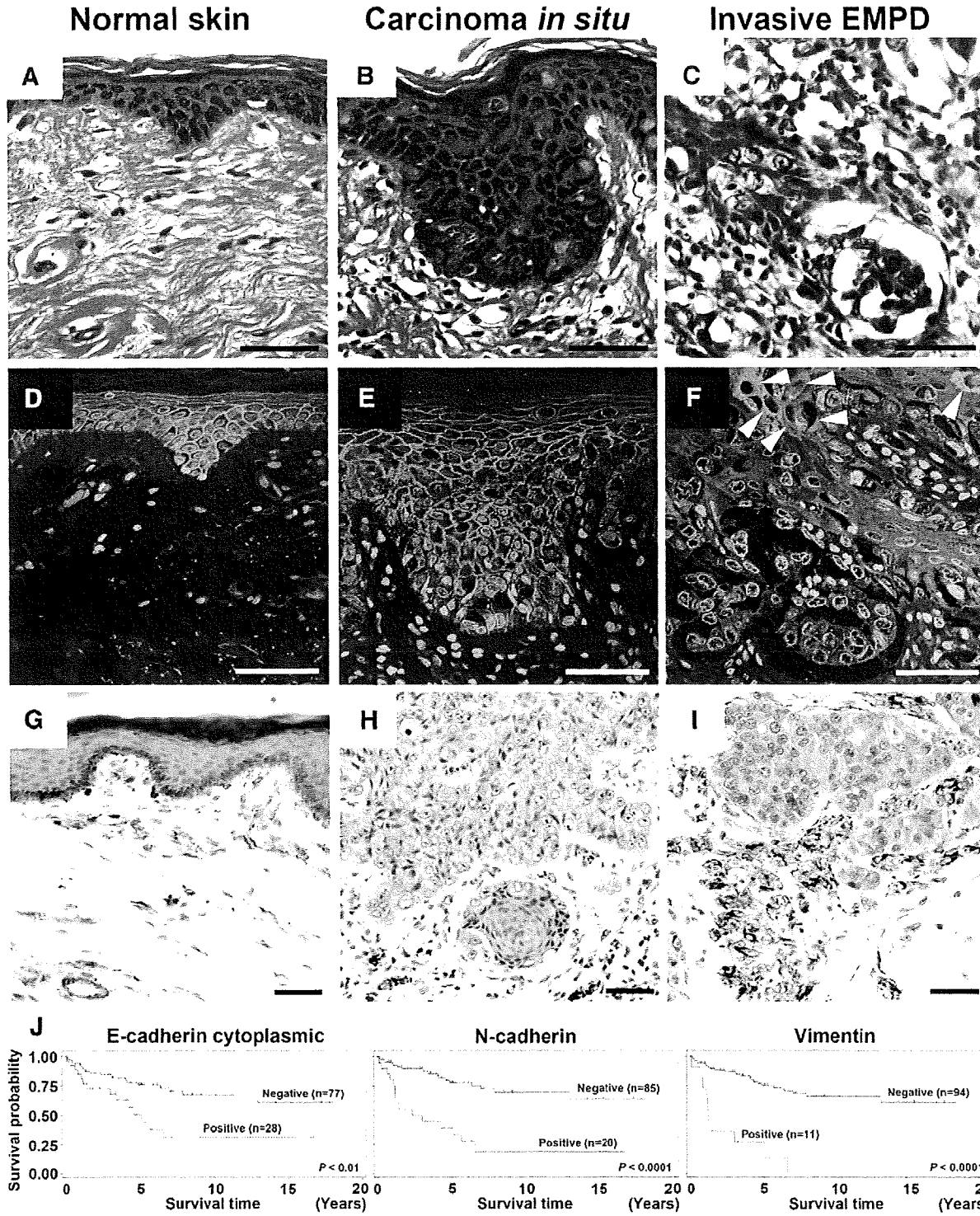

Figure 3. Epithelial-mesenchymal transition-like phenotypes as novel prognostic parameters for reduced survival in EMPD. **A–C:** H&E staining of representative normal skin (**A**), CIS (**B**), and invasive EMPD tumors (**C**). **D–F:** Double-immunofluorescence staining for E-cadherin (green) and for N-cadherin (red) shows typical E-cadherin expression on the surface of normal epidermal keratinocytes (**D**). In contrast, intraepidermal Paget cells do not express high levels of E-cadherin (**E**). Cytoplasmic E-cadherin expression is obvious in invasive EMPD tumors (**F, arrowheads**). The mesenchymal marker N-cadherin is induced in invasive Paget cells (**F**). **G–I:** Immunohistochemical staining shows vimentin expression in highly invasive Paget cells from patients with advanced disease (**I**, red) but not in normal epidermis (**G**) or CIS (**H**), suggesting that EMT-like phenotypes correlate with invasive feature of Paget cells. **J:** Kaplan-Meier survival analyses shows that the EMT-related markers N-cadherin and vimentin, and cytoplasmic E-cadherin expression are significantly associated with poor survival in EMPD. Scale bars = 50 μm (**A–I**). Nuclei are stained blue (DAPI or hematoxylin stain).

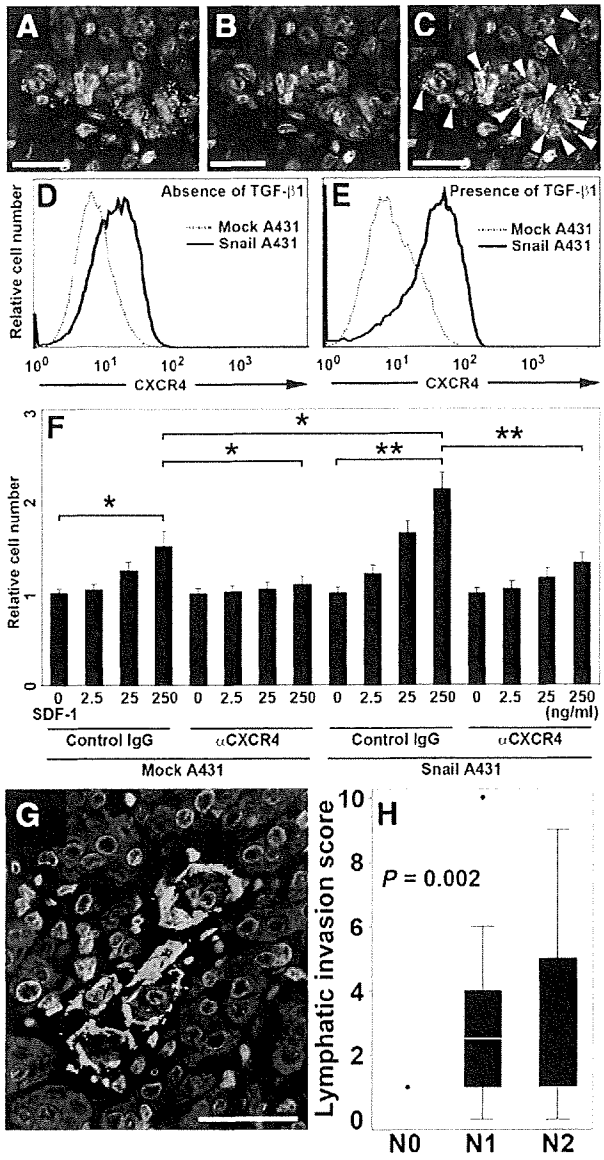

Figure 4. EMT-like process induces CXCR4 on A431 epidermoid cells and enhances their chemotaxis to SDF-1. **A–C:** CXCR4 expression (**B**, red) in invasive Paget cells detected in N-cadherin-positive cells (**A**, green; **C**, yellow, **arrowheads**). **D:** Expression of CXCR4 is considerably increased on the surface of A431 cells transfected with Snail as compared with mock-transfected A431 cells. **E:** TGF-β1 further induced expression of CXCR4 on Snail- but not mock-transfected A431 cells, indicating that EMT-like process promotes CXCR4 induction in vulval epidermoid tumor cell lines. **F:** Chemotaxis by TGF-β1-treated Snail-transfected A431 cells in upper chambers is enhanced toward SDF-1 in the bottom chambers as compared with mock-transfected A431 cells. Neutralization of CXCR4 on A431 cells significantly inhibited enhanced chemotaxis to SDF-1, suggesting that the CXCR4-SDF-1 axis is necessary to promote motility of A431 cells undergoing EMT-like process. Data are expressed as means ± SD; $^{*}P < 0.05$ and $^{**}P < 0.01$. **G:** Double immunofluorescence staining shows lymphatic invasion by cytokeratin 7-positive Paget cells (red) within tumor-associated lymphatic vessels (green). **H:** Multivariable linear regression analysis shows that increased lymphatic invasion in primary tumors statistically correlates with progression of nodal status in metastatic EMPD ($P = 0.002$). Lymphatic invasion was significantly increased at stages N1 and N2 as compared with N0 ($P = 0.002$ and 0.003, respectively). Scale bars: **A–C**, 30 μm; **G**, 25 μm.

with invasive EMPD to determine whether active invasion of lymphatic vessels by Paget cells is induced by EMT-like features and/or CXCR4 and to predict the subsequent incidence of regional LN metastasis. Double-immunofluorescence staining for cytokeratin 7 (expressed by tumor cells) and for podoplanin identified active invasion of the tumor-associated lymphatic vessels by Paget cells (Figure 4G). Expression of the EMT-related markers vimentin and N-cadherin, and of cytoplasmic E-cadherin, closely correlated with the incidence of lymphatic invasion in primary skin tumors ($P = 0.0003$, 0.0036, and 0.012, respectively). Furthermore, expression of CXCR4 was strongly associated with the incidence of lymphatic invasion within the primary sites ($P < 0.0001$). Importantly, presence of those EMT-associated markers closely correlated with the expression of CXCR4 by invasive Paget cells ($P < 0.01$, respectively), revealing a potential induction of CXCR4 by EMT-related process in invasive Paget cells. Moreover, lymphatic invasion by Paget cells was significantly increased at stages N1 and N2, compared with N0 ($P = 0.002$ and 0.003, respectively; Figure 4H). Multivariable linear regression analysis adjusted for age and gender confirmed a remarkable increase of lymphatic invasion throughout N-grade progression ($P = 0.002$; Figure 4H). Taken together, these results indicate that EMT-related features actively promote tumor cell invasion into tumor-associated lymphatic vessels, and that active lymphatic invasion by Paget cells undergoing EMT-like process probably promotes the successive progression of regional LN metastasis, leading to an increased risk for patient survival in EMPD.

Enhanced Nodal Lymphangiogenesis in Regional LNs during Tumor Metastasis

We and others[18,20,44] have shown in experimental animal tumor models that primary tumors can promote metastatic spread by the induction of lymphangiogenesis within draining lymph nodes. Therefore, to investigate whether nodal LECs are involved in human EMPD metastasis, we assessed lymphangiogenesis and the formation of a pre-metastatic niche within regional LNs. Lymphangiogenesis in LNs containing metastatic Paget cells was obviously induced within the metastases (Figures 5C and 6, A and B). Surprisingly, lymphatic vessel growth in regional LNs was already induced in patients with invasive EMPD before the tumors had metastasized (Figure 5B), whereas such changes were undetectable in the regional LNs of patients with CIS (Figure 5A). Quantitative image analysis of LN sections stained for podoplanin and von Willebrand factor and logistic regression analysis confirmed that lymphatic vessel growth within the regional LNs was progressively enhanced throughout the metastatic process ($P < 0.001$; Figure 5D). Computer-assisted morphometric analysis revealed that areas of lymphatic vessels in the LNs of group N1 and N2 tumors ($n = 19$) were significantly more extensive than in the group with N0 ($n = 14$) tumors ($P = 0.022$). Taken together, these results suggest that the activation of tumor-associated sinusoidal lymphatic vessels is induced before metastasis, and enhanced by metastatic Paget cells within regional LNs.

Therefore, we investigated whether increased lymphatic vessel areas (LVAs) in regional LNs could predict

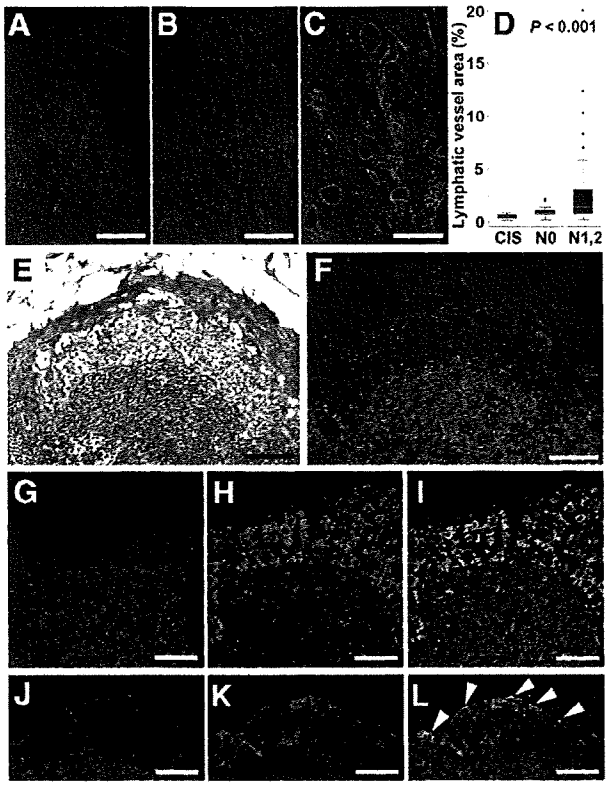

Figure 5. Lymphvascular niche within the regional LNs in patients with EMPD. **A–C:** Double-immunofluorescence staining shows enlarged tumor-associated lymphatic vessels in metastatic regional LNs (**C**, green). New lymphatic vessel growth is already induced before tumor metastasis (**B**, green). Vasculature in normal LNs visualized using anti-von Willebrand factor antibody for blood vessels (**A**, red) and D2–40 for lymphatic vessels (**A**, green). **D:** Progressive lymphatic vessel growth within regional LNs during metastatic process was confirmed by linear regression analysis ($P < 0.001$). Data are expressed as means ± SD. **E:** Subcapsular sinus of nonmetastatic regional LNs draining EMPD tumor (H&E stain). **F:** Immunofluorescence staining shows SDF-1 expression in subcapsular sinus. **G–I:** Immunofluorescence staining using macrophage marker HAM56 (**H**, green) shows that macrophages within subcapsular sinus (**I**, yellow) express high levels of SDF-1 (**G**, red). **J–L:** Podoplanin-positive lymphatic sinusoidal cells (K, green) express SDF-1 in subcapsular sinus (**J**, red; **L**, yellow, **arrowheads**). Nuclei are stained blue (DAPI stain). Scale bars = 100 (**A–C**, **E**, and **F**) and 50 (**G–L**) μm.

distant LN metastasis. We found that LVAs in regional LNs were increased in patients with distant LN metastasis (LVA without versus with regional LN metastasis; 0.88 ± 1.26% versus 3.10 ± 3.50%; $P = 0.1204$), indicating that lymphatic vessel enhancement in regional LNs could predict the presence of distant LN metastasis.

We also found that sinusoidal LECs and macrophages within the subcapsular sinuses of non-metastatic regional LNs draining EMPD tumors expressed abundant SDF-1 (Figure 5, E–L). Thus, the subcapsular sinuses that comprise primary sites of tumor metastasis in the LNs might form premetastatic niches[45,46] by promoting the migration and retention of CXCR4-positive Paget cells. In fact, 8 of 9 and 6 of 11 patients had bilateral and unilateral regional LN metastases, respectively, but Paget cells in primary invasive tumors expressed high levels of CXCR4 in only 2 of 95 patients without regional LN metastases. Importantly, CXCR4 was expressed within primary sites in 13 of 15 patients with distant LN metastasis. Indeed, distant LN metastasis was significantly associated with CXCR4 expression by invasive Paget cells in primary tumors, compared with its absence ($P < 0.0001$). Therefore, these results suggest that the CXCR4-SDF-1 axis contributes to the increase of distant LN metastasis in EMPD.

Lymphatic Invasion within Regional LNs Predicts Distant LN and Organ Metastasis

We previously showed in mouse models of experimental carcinogenesis that LN lymphangiogenesis, which might be a target for metastatic tumor cells, positively mediates distant LN and distant organ metastasis.[18,20] Therefore, we examined nodal lymphangiogenesis and metastatic Paget cells within tumor-associated lymphatic vessels in the regional LNs of 23 patients with dermal invasion in primary sites. Routine histology stains revealed metastatic tumor cell foci within the regional LNs but tumor cell-lymphatic vessel interactions could not be analyzed in detail (Figure 6A). Immunofluorescence stains for podoplanin and von Willebrand factor demonstrated not only new lymphatic vessel growth within the regional LNs (Figure 6B), but also the presence of metastatic Paget cells within these metastasis-associated lymphatic vessels (Figure 6, C and D).

Therefore, we investigated Paget cell invasiveness toward tumor-associated sinusoidal lymphatic vessels within regional LNs. We examined the expression of cytokeratin 7 in metastatic Paget cells and in sinusoidal lymphatic vessels by double-immunofluorescence staining (Figure 6, E and F). Lymphatic invasion by Paget cells within regional LNs significantly correlated with distant LN metastasis (metastasis in distant LN(s) beyond regional LN(s), $n = 12$) ($P = 0.0472$; Figure 6G) and with visceral organ metastasis (metastasis in visceral organs, $n = 11$) ($P = 0.0033$; Figure 6H). We also found that distant LN metastasis was a significant prognostic parameter for reduced overall survival in patients with EMPD ($P = 0.0004$; Figure 6H). Taken together, these findings indicate that lymphatic invasion within regional LNs promotes distant LN and organ metastasis in patients with EMPD and leads to a poor outcome.

Discussion

The present study analyzed the largest cohort of patients with EMPD known to date, and identified novel pathomechanisms that promote regional and distant LN metastasis. Tumor lymphangiogenesis was induced not only in primary tumors, but also in regional LNs draining invasive EMPD tumors. Our results revealed that lymphatic invasion by metastatic Paget cells in regional LNs indicate a high risk of distant metastasis and of poor survival for patients with EMPD. Invasion of metastasis-associated lymphatic vessels by Paget cells within regional LNs significantly correlated with distant LN and distant organ metastasis, indicating that active lymphatic invasion in regional LNs is a novel risk marker for the systemic

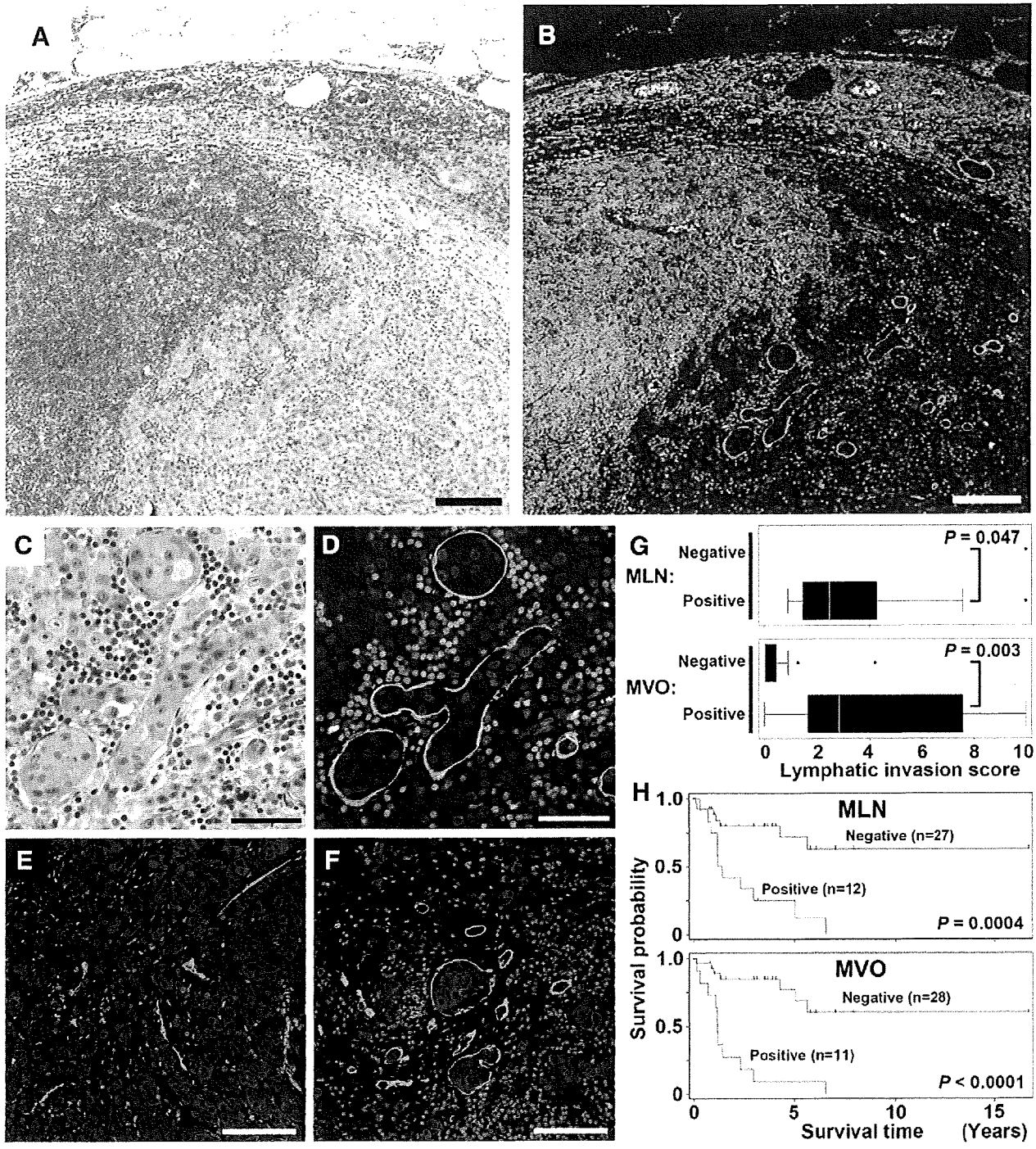

Figure 6. Lymphatic invasion within regional LNs is associated with distant LN metastasis. **A:** Routine H&E stains of metastatic regional LNs. Normal LN structure is visible on left side. Metastatic Paget cells occupy right side of LN. Tumor-associated nodal lymphangiogenesis was detected by immunofluorescence staining for podoplanin (**B**, green), as compared with nonmetastatic regions of LN. **C** and **D:** High power magnification of metastatic LNs confirms that metastatic Paget cells invade podoplanin-positive lymphatic vessels. Blood vessels stained red for von Willebrand factor (**B** and **D**). Double-immunofluorescence staining of metastatic regional LNs for cytokeratin 7 (red) and for podoplanin (green) with poor (**F**) or successful (**E**) clinical outcome. Metastatic Paget cells were identified in regional LNs using anti-cytokeratin 7 antibody, whereas these Paget cells did not invade tumor-associated podoplanin-positive lymphatic vessels (**E**). In contrast, highly aggressive Paget cells invaded adjacent lymphatic vessels (**F**), likely enabling them to further metastasize beyond regional LNs. Nuclei are stained blue (DAPI stain). Scale bars = 100 (**A**, **B**, **E**, and **F**) and 50 (**C** and **D**) mm. **G:** Lymphatic invasion scores within regional LNs are significantly increased in patients with distant LN (MLN; $n = 12$) or visceral organ (MVO; $n = 11$) metastasis compared with those without metastasis ($P = 0.047$ and $P = 0.003$, respectively). Data are expressed as means ± SD. **H:** Distant LN metastasis/MLN is significantly associated with reduced patient survival (Kaplan-Meier survival analyses; $P = 0.0004$). MLN, metastasis in distant LN(s) beyond regional LN(s); MVO, metastasis in visceral organs (lung, liver, bone).